

# Towards a Solution to the $H_0$ Tension: the Price to Pay

Axel de la Macorra,<sup>a</sup> Erick Almaraz<sup>b</sup> and Joanna Garrido<sup>a</sup>

<sup>a</sup>Instituto de Física, Universidad Nacional Autónoma de México,  
Circuito de la Investigación Científica Ciudad Universitaria, 04510 CDMX, México

<sup>b</sup>African Institute for Mathematical Sciences AIMS, Cape Town, South Africa

E-mail: [macorra@fisica.unam.mx](mailto:macorra@fisica.unam.mx), [ealmaraz@gmail.com](mailto:ealmaraz@gmail.com),  
[joannagarr@ciencias.unam.mx](mailto:joannagarr@ciencias.unam.mx)

**Abstract.** The tension between current expansion rate  $H_0$  using Planck data and direct model-independent measurements in the local universe has reached a tension above  $5\sigma$  in the context of the  $\Lambda$ CDM model. The growing tension among early time and local measurements of  $H_0$  has not ameliorated and remains a crucial and open question in cosmology. Solutions to understand this tension are possible hidden sources of systematic error in the observable measurements or modifications to the concordance  $\Lambda$ CDM model. In this work, we investigate a solution to the  $H_0$  tension by modifying  $\Lambda$ CDM and we add at early times extra relativistic energy density  $\rho_{ex}$  beyond the Standard Model. For scale factor larger than  $a_c$  this extra energy density  $\rho_{ex}$  dilutes faster than radiation and becomes subdominant. In some context this  $\rho_{ex}$  corresponds to Early Dark Energy (EDE) or by Bound Dark Energy (BDE) and we refer to this cosmological model as  $\Lambda$ CDM-Nx. We implement  $\Lambda$ CDM-Nx in CAMB and perform a full COSMO-MC (MCMC) allowing to simultaneously fit the latest data from CMB anisotropies and the value of  $H_0 = 74.03 \pm 1.42, \text{ km s}^{-1} \text{ Mpc}^{-1}$  obtained by distance ladder measurements using Cepheid variables to calibrate the absolute luminosity of Type Ia supernovae by A. Riess [R-19] [1]. The inclusion of  $\rho_{ex}$  ameliorates the tension between early and late time measurements only slightly and we obtain a value  $H_0 = (68.70 \pm 0.45 \text{ km s}^{-1} \text{ Mpc}^{-1})$  still in conflict with local measurements [R-19]. We follow up our analysis by proposing two forecasting standard deviation  $\sigma_H = 1$  and  $\sigma_H = 0.5$  (in units of  $\text{km s}^{-1} \text{ Mpc}^{-1}$ ) for local distance measurements, i.e.  $H_0 = (74.03 \pm 1) \text{ km s}^{-1} \text{ Mpc}^{-1}$  and  $H_0 = (74.03 \pm 0.5) \text{ km s}^{-1} \text{ Mpc}^{-1}$ . We implement these new values of  $H_0$  in MCMC and we obtain a value of  $H_0 = (72.83 \pm 0.47) \text{ km s}^{-1} \text{ Mpc}^{-1}$  at 68% confidence level for  $\sigma_H = 0.5$ , fully consistent with [R-19], while the price to pay is a percentage increase of 0.12% in CMB  $\chi^2_{cmb}$ . Finally, the extra energy density  $\rho_{ex}$  leaves distinctive imprints in the matter power spectrum at scales  $k \sim k_c$  with  $k_c = a_c H(a_c)$  and in the CMB power spectrum, allowing for independent verification of our analysis.

**Keywords:**  $H_0$ , Hubble Tension, Early Dark Energy

---

<sup>1</sup>Corresponding author

---

## Contents

<b>1</b>	<b>Overview</b>	<b>1</b>
<b>2</b>	<b>Introduction</b>	<b>3</b>
<b>3</b>	<b>Cosmological Toy Models</b>	<b>5</b>
3.1	Acoustic Scale	5
3.2	Impact of $\rho_{ex}$ on the Acoustic Scale $r_s(a_*)$	8
3.3	Matter Power Spectrum and $\rho_{ex}$	9
<b>4</b>	<b>Cosmological Results and MCMC implementation</b>	<b>10</b>
4.1	Analysis	13
4.2	Matter Power Spectrum and CMB Power Spectrum	18
<b>5</b>	<b>Conclusions</b>	<b>18</b>

---

## 1 Overview

Even before the discovery of the accelerated expansion rate of the Universe [2–4], the quest for determining the rate of expansion of the Universe has occupied a central role in cosmology for decades. However, great technical and observational achievements in recent years have delivered percentage-level precision measurements of the cosmological parameters. The improvement probing the physics of different epochs of the universe has yielded discordance in some measurements. In particular we have an increasing tension among the value of some cosmological parameters as for example the value of  $H_0$ .

According to the distance ladder measurements, which uses close by Cepheids to anchor supernovae data and determine their distance [1, 5, 6], the obtained value for the Hubble parameter is up to  $3.4\sigma$  higher than the value determined using Cosmic Microwave Background (CMB) probes. This distance ladder method to determine  $H_0$  is model-independent, i.e. it does not rely on the underlying cosmological model, and the latest estimated reports a value of  $H_0 = 74.03 \pm 1.42 \text{ km s}^{-1}\text{Mpc}^{-1}$  [1].

An alternative calibration of the distance ladder uses the tip of the red giant branch (TRGB) method [7]. This method is independent of the Cepheid distance scale and gives a value of  $H_0 = 69.8 \pm 1.9 \text{ km s}^{-1}\text{Mpc}^{-1}$  [8] which is midway in the range defined by the current Hubble tension. It agrees at the  $1.2\sigma$  level with that of the Planck collaboration [9], and at the  $1.7\sigma$  level with the  $SH_0ES$  (Supernovae  $H_0$  for the Equation of State) measurement of  $H_0$  based on the Cepheid distance scale [1]. Measurements of lensing time delays [10–12] between multiple images of background quasars provide a high value for  $H_0$  which is in agreement with the traditional local distance ladder estimation. In [10] they report a value of  $H_0 = 71.9^{+2.4}_{-3.0} \text{ km s}^{-1}\text{Mpc}^{-1}$ , while [11] finds a value  $H_0 = 72.5^{+2.1}_{-2.3} \text{ km s}^{-1}\text{Mpc}^{-1}$ , and the  $H0LiCOW$  ( $H_0$  Lenses in CosmoGrail Wellspring) team [12], reports  $H_0 = 73.3^{+1.7}_{-1.8} \text{ km s}^{-1}\text{Mpc}^{-1}$ , by making a joint analysis of six gravitationally lensed quasars with measured time delays. This technique is completely independent of both the supernovae and CMB analyses.

The precise CMB measurements by Planck [P-18] determines a value of the Hubble parameter as  $H_0 = (67.27 \pm 0.60) \text{ km s}^{-1}\text{Mpc}^{-1}$  at 68% confidence level assuming the standard

$\Lambda$ CDM model, corresponding the particle content of the standard model of particles physics [13] supplemented by cold dark matter and a cosmological constant as dark energy. The value of  $H_0$  from CMB is in conflict with the value of  $H_0$  determined at late cosmological times from local measurements in Riess et al [R-19] [1] given by  $H_0 = (74.03 \pm 1.42) \text{ km s}^{-1} \text{ Mpc}^{-1}$  and with an average reported value  $H_0 = (73.3 \pm 0.8) \text{ km s}^{-1} \text{ Mpc}^{-1}$  [14] from different local measurements projects. A combined analysis of distance measurements for four megamaser-hosting galaxies done by the Megamaser Cosmology Project (MCP) [15] reports a value  $H_0 = 73.9 \pm 3.0 \text{ km s}^{-1} \text{ Mpc}^{-1}$ . A combination of time-delay cosmography and the distance ladder results is in  $5.3\sigma$  tension with Planck CMB determinations of  $H_0$  in flat  $\Lambda$ CDM.

On the other hand, the latest results from the Planck collaboration report a model dependent  $\Lambda$ CDM extrapolated value of  $H_0 = (67.36 \pm 0.54) \text{ km s}^{-1} \text{ Mpc}^{-1}$  [9], while the latest results the Atacama Cosmology Telescope [16] CMB probe found a value that agrees with the Planck satellite estimate within 0.3%, reporting a value of  $H_0 = 67.6 \pm 1.5 \text{ km s}^{-1} \text{ Mpc}^{-1}$ . In a recent review L.Verde, A. Riess and T.True reported an average value of local measurements of  $H_0 = 73.03 \pm 0.8 \text{ km s}^{-1} \text{ Mpc}^{-1}$  [14]. Regardless of the exact value of  $H_0$  by local measurements, the significance of the tension between the measurements of early and late time lies in the range  $4.0\sigma$  and  $5.7\sigma$  [14], implying some profound miss-understanding in either the systematic errors of the observational analysis, or the theoretical  $\Lambda$ CDM model.

The discrepancy between the early and late-Universe  $H_0$  measurements has gained major attention by the cosmological community and some authors have explored a variety of extensions to the minimal  $\Lambda$ CDM model to accommodate the high value of  $H_0$  obtained by local measurements with the precise information encoded in the CMB. Trying to understand the tension between these two values led to a reexamination of possible sources of systematic errors in the observations [17], [18], [19], but it also suggests the need to extend our physical model describing the universe. Any of these theoretical modifications should leave the accurate determination of the angular scale of the acoustic peaks in the CMB power spectrum by Planck unchanged [20].

The  $H_0$  tension has been studied recently in [21–25] and more recently in [26–33] where the impact on structure formation has been studied.

The suggestion made by [5] to explore the existence of dark radiation in the early Universe in the range of  $\Delta N_{eff} = 0.4 - 1$  to solve this tension was explored in detail by [34] where they explore changing the value of  $N_{eff}$  and  $c_s$ . Alternatively, some models explore the possibility of having interactions between the dark sector that can, not only help to solve the cosmic coincidence problem but also solve the  $H_0$  tension [35, 36]. In the logic of exploring alternative models for the dark sector, in [37] investigated the possible scenarios for a phantom crossing dark energy component as another option for solving the Hubble tension. Given the amount of interest invested in this topic, some authors have explored changes to General Relativity in order to accommodate the high value of  $H_0$  with CMB data. For instance, the work by [38] explores a model in which a fifth force between dark matter particles is mediated by a scalar field which plays the role of dark energy. In another work, models which vary the effective gravitational constant and effective number of relativistic degrees of freedom are explored by [39]. In a different approach, [40] explores the possibility of strongly interacting massive neutrinos to alleviate the  $H_0$  tension.

However, perhaps the most widely explored extension to  $\Lambda$ CDM is known as Early Dark Energy (EDE) [41–44]. There is no unique or unambiguous definition of EDE. Typically in EDE models there is an early period during which an extra energy component, not contained in  $\Lambda$ CDM model, contributes to the expansion rate of the universe  $H$ . Even the terminology

of "early period" is model and case dependent as it can take place in radiation domination era or at late times as for example at  $z \sim 4$ . Original Early Dark Energy models were motivated by the evolution of scalar fields (quintessence) to describe the evolution of Dark Energy [41, 42, 45–47]. These EDE models had in general a non-negligible energy density at early times well in radiation domination. The equation of state  $w$  of the quintessence scalar field had a period of  $w = 1/3$  at early times with a later transition to  $w \sim 1$ , diluting the energy density and becoming subdominant for a long period of time covering most of the matter domination period, to finally reappear dynamically at late time as dark energy and were originally studied in [48, 49] and [50–53] and [54, 55]. Alternatively, recent EDE models add an extra component to the energy-momentum tensor  $\Omega_{\text{EDE}}(a)$  at different scales and this EDE dilutes rapidly at scale factor  $a_c$ , which determines the time of the transition, with  $\Omega_{\text{EDE}} = 0$  for  $a \gg a_c$ . This EDE modifies the expansion rate of the universe, the cosmological distances and the density perturbations at different epochs [43, 56] and [21, 57, 58] and have been proposed as deviations from  $\Lambda$ CDM and possible solutions to  $H_0$  crisis [1].

Furthermore, the increasing statistical tension in the estimated Hubble parameter from early and late times observations [14] has reignited interest in alternative cosmological models, while the surge in clustering data [59] and the percentage precision for cosmic distances [9, 59] allows to search for extensions beyond  $\Lambda$ CDM by searching for cosmological features in the matter [24, 32, 42, 43, 56, 57, 60] or CMB power spectra, standard distances rulers, or tensions in  $\Lambda$ CDM model as the recent  $H_0$  crisis [1].

On the other hand a physically motivated Dark Energy model presented in [51, 61–63] introduces a dark sector, corresponding to a dark gauge group  $SU(3)$  similar to the strong QCD interaction in the standard model. The fundamental particles contained in this dark  $SU(3)$  are massless and redshift as radiation for  $a < a_c$  but the underlying dynamics of the gauge interaction of this group forms massive bound states once the interaction becomes strong, similar as with protons and neutrons in the strong QCD force, and we refer to this model as "Bound Dark Energy model" (BDE) [51, 61, 62]. The energy of the elementary particles is transferred to the lightest bound state after the phase transition takes place at  $a_c$  and corresponds to a scalar field  $\phi$ . Due to the dynamics of  $\phi$  the energy density of BDE dilutes at  $a_c$  and eventually reappears close to present time as Dark Energy [61, 62]. This dilution at  $a_c$  leaves interesting imprints on the matter power spectrum [63] (for a model independent analysis see for instance [64, 65]). BDE is a particular model of elementary particles physics where an extra gauge group  $SU(3)$  is introduced and contains naturally the main characteristics of EDE, namely it accounts for extra relativistic energy density  $\rho_{ex}$  at high energies while  $\rho_{ex}(a)$  dilutes rapidly for  $a > a_c$  due to a phase transition of the underlying gauge and forms bound states [61, 62].

The main goal in this work is study the tension and possible solution in the value of  $H_0$  from low redshift probes with the precise determination of CMB data. This paper is organised as follows. Section 2 we present a brief introduction and the details behind our modifications through a toy model calculations in section 3. The working details and implementation in the Boltzmann code CAMB and COSMOMC are presented in section 4, the results are discussed in section 4 and the analysis are in section 4.1, while we present our conclusions in 5.

## 2 Introduction

The main goal in this work is study the tension and possible solutions in the value of  $H_0$  from low redshift probes and the precise determination of CMB data. We work with two different

cosmological models, the first one is simply the standard  $\Lambda$ CDM model, corresponding to a content of the standard model of particles physics [13], cold dark matter and a cosmological constant as dark energy, while the second model we denote as  $\Lambda$ CDM-Nx, corresponding to  $\Lambda$ CDM but supplemented with extra relativistic energy density  $\rho_{ex}(a) \sim 1/a^3$  present at a scale factor  $a \leq a_c$ , while for  $a > a_c$   $\rho_{ex}(a)$  dilutes as  $\rho_{ex}(a) \sim 1/a^6$ . This model  $\Lambda$ CDM-Nx is inspired by BDE [61, 62].

For definiteness in this study we take the recent local measurement  $H_0 = (74.03 \pm 1.42) \text{ km s}^{-1} \text{ Mpc}^{-1}$  at 68% confidence level from Riess et al [R-19] [1], and the inferred value of  $H_0 = (67.27 \pm 0.60) \text{ km s}^{-1} \text{ Mpc}^{-1}$  at one- $\sigma$  level from Planck-2018 [Pl-18] [9] for a  $\Lambda$ CDM model using (TT,TE,EE+LowE) measurements. We modified CAMB [66, 67] and make a full COSMO-MC (Markov Chains) analysis<sup>1</sup> [68–70]. We perform the analysis for  $\Lambda$ CDM and  $\Lambda$ CDM-Nx models. However, besides the one-sigma value  $\sigma_H = 1.42$  from local  $H_0$  measurements [R-19] and we also consider two forecasting one-sigma values  $\sigma_H$ , and for definiteness we choose and we introduce in the analysis a value of  $H_0 = (74.03 \pm \sigma_H) \text{ km s}^{-1} \text{ Mpc}^{-1}$  with  $\sigma_H = 1$  and  $\sigma_H = 0.5$  (in units of  $\text{km s}^{-1} \text{ Mpc}^{-1}$ ). With these two forecasting values we asses the impact of a more precise local  $H_0$  measurements on the posterior value of  $H_0$  from CMB + local  $H_0$  data. Notice however, that our forecasting one-sigma  $\sigma_H = 1$  and  $\sigma_H = 0.5$  are similar to the one reported in [14] with  $H_0 = (73.03 \pm 0.8) \text{ km s}^{-1} \text{ Mpc}^{-1}$ . The results of our analysis are shown in section 4.1 and we present the conclusions in (5).

The value of  $H_0 = 74.03 \pm 1.42 \text{ km s}^{-1} \text{ Mpc}^{-1}$  measurements determined by A. Riess and his team [R-19] [1, 5, 6] has a discrepancy between  $4.0\sigma$  and  $5.8\sigma$  [14] with the Planck’s CMB (TT,TE,EE+LowE) [9] [P-18] inferred value of  $H_0 = (67.27 \pm 0.60) \text{ km s}^{-1} \text{ Mpc}^{-1}$  at one- $\sigma$  level in a  $\Lambda$ CDM model. The solution to this discrepancy remains an open question in cosmology. Since CMB radiation is generated at an early epoch  $a_\star = 1/1090$ , the prediction of the Hubble constant at present time  $H_0$  inferred by Planck data is a consequence of the assumption of the validity of the standard  $\Lambda$ CDM model. So either Planck or local  $H_0$  measurements are inaccurate, due to possible systematics, or we need to modify the concordance cosmological  $\Lambda$ CDM model. Here we follow this second option and we will attempt to reconcile the value of  $H_0$  of these two observational experiments.

We will work with two different cosmological models. The first one is simply the standard  $\Lambda$ CDM model, corresponding to a content of the standard model (sm) particles physics [13] and a cosmological constant as dark energy. We name the second model as  $\Lambda$ CDM-Nx and it consists of  $\Lambda$ CDM supplemented by an extra relativistic energy density  $\rho_{ex}(a) \sim 1/a^3$  present at early times for a scale factor  $a \leq a_c$ , where  $a_c$  denotes the transition scale factor, and we assume that  $\rho_{ex}(a) \sim 1/a^6$  for  $a > a_c$ , motivated by BDE and EDE models.

We have implemented the cosmological  $\Lambda$ CDM-Nx model in CAMB [66, 67] and and we perform a full COSMO-MC (Markov Chains) analysis for several data sets described in section (sec.results) for both  $\Lambda$ CDM and  $\Lambda$ CDM-Nx models and we present the results and conclusions in section (4).

For definiteness we take the (TT,TE,EE+lowE) measurements from Planck-2018 [Pl-18] [9] with  $H_0 = (67.27 \pm 0.60) \text{ km s}^{-1} \text{ Mpc}^{-1}$  and the recent local measurement  $H_0 = (74.03 \pm 1.42) \text{ km s}^{-1} \text{ Mpc}^{-1}$  at 68% confidence level from Riess et al [R-19] [1]. However, besides the one-sigma value  $\sigma_H = 1.42$  (in units of  $\text{km s}^{-1} \text{ Mpc}^{-1}$ ) from local measurements [R-19], we also introduce two forecasting one-sigma values and we choose  $\sigma_H = 1$  and  $\sigma_H = 0.5$ . With

---

<sup>1</sup><http://cosmologist.info/cosmomc>

these two forecasting values we want to assess the impact a more precise local  $H_0$  measurements on the posterior value of  $H_0$  combined with the same CMB as before. Notice however, that our forecasting one-sigma values  $\sigma_H = 1$  and  $\sigma_H = 0.5$  are of the same order as in the average value  $H_0 = (73.03 \pm 0.8) \text{ km s}^{-1} \text{ Mpc}^{-1}$  reported in [14]. The results of these analysis are shown in section 4.1 and we present the conclusions in (5).

Before discussing the results of the implemented the cosmological models  $\Lambda$ CDM and  $\Lambda$ CDM-Nx models in CAMB and COSMO-MC presented in section 4 we would like to follow up a simple toy model presented in in section 3 illustrating how an extra relativistic energy density  $\rho_{ex}(a)$ , present only at early times  $a < a_c$ , can account for the same acoustic scale  $\theta(a_*)$  as measured by Planck [P-18] but with the value of  $H_0$  consistent with Riess [R-19]. We estimate the cosmological constraints analytically in section 3.2 and we study the impact of the extra  $\rho_{ex}$  in the growth of the linear matter density and in the matter power spectrum in section 3.3.

### 3 Cosmological Toy Models

We present now a simple toy model illustrating analytically how adding an extra relativistic energy density  $\rho_{ex}(a)$ , present at early times, can account for having the same acoustic scale  $\theta(a_*)$  as  $\Lambda$ CDM model but with a higher value of  $H_0$ .

#### 3.1 Acoustic Scale

Planck satellite [9] has delivered impressive quality cosmological data by measuring the CMB background radiation. Perhaps the most accurate measurements is the acoustic scale anisotropies given by the acoustic angle  $\theta$  defined in as the ratio of the comoving sound horizon  $r_s(a_*)$  and the comoving angular diameter distance  $D_A(a_*)$  evaluated at recombination scale factor  $a_*$  (with a redshift  $z_* = 1/a_* - 1 \simeq 1089$ ) as

$$\theta(a_*) = \frac{r_s(a_*)}{D_A(a_*)}. \quad (3.1)$$

The (TT,TE,EE+lowE) CMB Planck-2018 [9] measurements at 68% confidence level gives

$$100 \theta(a_*) = (1.04109 \pm 0.0003), \quad (3.2)$$

in the context of the standard  $\Lambda$ CDM model, corresponding to a flat universe with cold dark matter (CDM), a cosmological constant  $\Lambda$  as dark energy and the Standard Model particles [13]. The comoving angular diameter distance and the acoustic scale are defined as

$$D_A(a_*) = \int_{a_*}^{a_o} \frac{da}{a^2 H(a)}, \quad r_s(a_*) = \int_{a_i}^{a_*} \frac{c_s}{a^2 H(a)} da \quad (3.3)$$

with  $H(a) \equiv \dot{a}/a$  the Hubble parameter and  $c_s$  the sound speed,

$$c_s(a) = \frac{1}{\sqrt{3(1+R)}}, \quad R \equiv \frac{3 \rho_b}{4 \rho_\gamma} = \frac{3}{4} \left( \frac{\Omega_{bo}}{\Omega_{\gamma o}} \right) \left( \frac{a}{a_o} \right). \quad (3.4)$$

Since Planck CMB measurements determines the angle acoustic  $\theta(a_*) = r_s(a_*)/D_A(a_*)$  accurately, any modification of  $\Lambda$ CDM must clearly preserved the ratio in  $\theta(a_*)$ . A larger value of  $H_0$  reduces  $D_A(a_*)$  and  $r_s(a_*)$ , however since the integrations limits differ in  $D_A(a_*)$  and  $r_s(a_*)$  a change in  $H_0$  will modify the angle  $\theta(a_*)$ .

Let us take two models, the standard  $\Lambda$ CDM model (or "sm") and  $\Lambda$ CDM-Nx (also referred as "smx") corresponding to a  $\Lambda$ CDM with additional relativistic particles for  $a < a_*$ . Imposing the constraint to have the same acoustic scale  $\theta(a_*)$  in these two models, i.e.

$$\theta(a_*) = \frac{r_s^{sm}(a_*)}{D_A^{sm}(a_*)} = \frac{r_s^{smx}(a_*)}{D_A^{smx}(a_*)}, \quad (3.5)$$

the relative quotient of  $r_s(a_*)$  and  $D_A(a_*)$  of these models must satisfy

$$\xi \equiv \frac{D_A^{smx}(a_*)}{D_A^{sm}(a_*)} = \frac{r_s^{smx}(a_*)}{r_s^{sm}(a_*)}. \quad (3.6)$$

Any change in  $D_A(a_*)^{smx}/D_A^{sm}(a_*)$ , due for example for a different amount of  $H_0$ , can be compensated with a change in  $r_s(a_*)^{smx}/r_s(a_*)^{sm}$  to maintain the same  $\theta(a_*)$ .

We impose the constraint to have the same acoustic scale  $\theta(a_*)$  in both models, with  $\Lambda$ CDM (i.e. "sm") having a value of  $H_0$  as measured by Planck-2018 [P18], where we take for presentation purposes  $H_0^P = 67$  (in units of  $\text{km s}^{-1}\text{Mpc}^{-1}$ ), and the second model  $\Lambda$ CDM-Nx (i.e. "smx"), corresponding to the standard  $\Lambda$ CDM model with extra relativistic energy density  $\rho_{ex}(a)$  and an  $H_0$  given by  $H_0^R = 74$  (in units of  $\text{km s}^{-1}\text{Mpc}^{-1}$ ), consistent with A. Riess et al [R19]. We define the Hubble parameter in  $\Lambda$ CDM as  $H_{sm}^2 = (8\pi G/3)\rho_{sm}$  with an energy content  $\rho_{sm} = \rho_r^{sm} + \rho_m^{sm} + \rho_\Lambda^{sm}$  for radiation, matter and cosmological constant, respectively, while  $\Lambda$ CDM-Nx has  $H_{smx}^2 = (8\pi G/3)\rho_{smx}$  with  $\rho_{smx} \equiv \rho_r^{smx} + \rho_m^{smx} + \rho_\Lambda^{smx}$ . For simplicity we assume the same amount of matter in both models and we take for model  $\rho^{smx}$  the following content:

- i) for  $a \leq a_c$  we have extra radiation  $\rho_{ex} \neq 0$  with  $\rho_r^{smx} = \rho_r^{sm} + \rho_{ex}$  and  $\rho_m^{smx} = \rho_m^{sm}$
- ii) for  $a > a_c$ , we have  $\rho_{ex} = 0$ ,  $\rho_r^{smx} = \rho_r^{sm}$ ,  $\rho_m^{smx} = \rho_m^{sm}$  but  $\rho_\Lambda^{smx} > \rho_\Lambda^{sm}$ .

We will now determine the relation between the amount  $\rho_{ex}(a_c)$  (or equivalently  $\Omega_{ex}(a_c)$ ) as a function of the transition scale  $a_c$  such that the ratio of the sound horizon  $r_s(a_*)$  at decoupling and the angular distance to the last scattering surface  $D_A(a_*)$  is unchanged, preserving thus the acoustic angle  $\theta(a_*)$  as measured by Planck [1], but with a Hubble parameter  $H_0$  in  $\Lambda$ CDM-Nx ("smx") model consistent with the high value of local measurements  $H_0^R = 74$  [1]. Taking  $H_0^{sm} = H_0^P = 67$  and  $H_0^{smx} = H_0^R = 74$  the ratio  $D_A^{smx}(a_*)/D_A^{sm}(a_*)$  gives

$$\xi = D_A^{smx}(a_*)/D_A^{sm}(a_*) = 0.981. \quad (3.7)$$

Since  $\xi < 1$  and using eq.(3.6) we require  $r_s^{smx}(a_*)/r_s^{sm}(a_*)$  to be smaller than one. We can achieve this by increasing  $H(a)$  in the region  $a \leq a_*$  in  $\Lambda$ CDM-Nx compared to the standard  $\Lambda$ CDM model by introducing extra radiation  $\rho_{ex}(a)$  in the region  $a < a_*$ . With this modification we tune  $\rho_{ex}(a_c)$  to obtain the ratio  $r_s^{smx}(a_*)/r_s^{sm}(a_*)$  to obtain the same value of  $\theta(a_*)$  in eq.(3.6) as measured by Planck-2018.

Let us compare the Hubble parameter in these two models in the region  $a \ll a_o$ , where dark energy is subdominant, giving

$$\frac{H_{sm}}{H_{smx}} = \sqrt{\frac{\rho_r^{sm} + \rho_m^{sm}}{\rho_r^{sm} + \rho_m^{sm} + \rho_{ex}}} = \sqrt{1 - \Omega_{ex}} \quad (3.8)$$

with

$$\Omega_{ex} \equiv \frac{\rho_{ex}}{\rho_{smx}} = \frac{\rho_{ex}}{\rho_{sm} + \rho_{ex}} \simeq \frac{N_{ex} \beta}{1 + (N_\nu + N_{ex}) \beta} \quad (3.9)$$

and the last term in eq.(3.9) is given in terms of relativistic degrees of freedom with  $\rho_{sm} = g_{sm}\rho_\gamma$ ,  $\rho_{ex} = g_{ex}\rho_\gamma$  and  $g_{sm} = 1 + N_\nu\beta$ ,  $g_{ex} = N_{ex}\beta$ ,  $g_{smx} = g_{sm} + g_{ex}$  with  $\rho_\gamma = \frac{\pi^2}{30} g_\gamma T_\gamma^4$ ,  $N_\nu = 3.046$  and  $N_{ex}$  the extra relativistic degrees of freedom in terms of the neutrino temperature and  $\beta = (7/8)(4/11)^{4/3}$ . Notice that last approximation in eq.(3.9) is only valid in radiation domination epoch. Since we assume in our toy models the same amount of matter and radiation in models  $\Lambda$ CDM and  $\Lambda$ CDM-Nx at present time but different values of  $H_0$ , we must necessarily have a larger amount of dark energy in model  $\Lambda$ CDM-Nx than in  $\Lambda$ CDM to account for the increase value in  $H_0$ . We constrain  $\Lambda$ CDM-Nx model by imposing that it gives same acoustic angle  $\theta(a_\star) = r_s(a_\star)/D_A(a_\star)$  as  $\Lambda$ CDM(c.f. eq.(3.5)) and relative quotient of  $r_s(a_\star)$  and  $D_A(a_\star)$  as in eq.(3.6).

We will now compare the Hubble parameter  $H$  in  $\Lambda$ CDM(sm) and  $\Lambda$ CDM-Nx(smx) models. By our working hypothesis both models have the same amount of matter and radiation at present time, while the value of  $H_0$  differs with  $H_0^P = 67$  for  $\Lambda$ CDM (sm) and  $H_0^R = 73$  for  $\Lambda$ CDM-Nx (smx). Let us express  $H$  as

$$H^{sm}(a) = H_0^{sm} \sqrt{\Omega_{mo}^{sm}(a/a_o)^{-3} + \Omega_{ro}^{sm}(a/a_o)^{-4} + \Omega_{\Lambda o}^{sm}} \quad (3.10)$$

and

$$H^{smx}(a) = H_0^{smx} \sqrt{\Omega_{mo}^{smx}(a/a_o)^{-3} + \Omega_{ro}^{smx}(a/a_o)^{-4} + \Omega_{\Lambda o}^{smx}} \quad (3.11)$$

with the constraint  $\Omega_{mo} + \Omega_{ro} + \Omega_{\Lambda o} = 1$  for both models. Since by assumption we have the same amount of matter and radiation,  $\rho_{mo}^{sm} = \rho_{mo}^{smx}$  and  $\rho_{ro}^{sm} = \rho_{ro}^{smx}$ , we simply multiply and divide by the critical density  $\rho_{co}$  of each model to get

$$\rho_{qo} = \Omega_{qo}^{sm} \rho_{co}^{sm} = \Omega_{qo}^{smx} \rho_{co}^{smx}, \quad \rho_{\Lambda o}^{smx} = \rho_{\Lambda o}^{sm} + \rho_{co}^{sm} \left( \frac{(H_0^{smx})^2}{(H_0^{sm})^2} - 1 \right) \quad (3.12)$$

with  $q = m, r$  for matter and radiation, respectively. Models  $\Lambda$ CDM (sm) and  $\Lambda$ CDM-Nx (smx) have the same  $\rho_{mo}$  and  $\rho_{ro}$  but a different amount of  $H_0$  gives a different amount of dark energy  $\rho_\Lambda$  as seen in eq. (3.12). We clearly see in eq.(3.12) how different amounts of  $H_0$  impacts the Dark Energy density in these two models. We further express

$$\Omega_{qo}^{smx} = \frac{(H_0^{sm})^2}{(H_0^{smx})^2} \Omega_{qo}^{sm}, \quad \Omega_{\Lambda o}^{smx} = 1 - (\Omega_{mo}^{smx} + \Omega_{ro}^{smx}) = 1 - \frac{(H_0^{sm})^2}{(H_0^{smx})^2} (\Omega_{mo}^{sm} + \Omega_{ro}^{sm}) \quad (3.13)$$

The Hubble parameter  $H$  becomes

$$H^s(a) = H_0^s \sqrt{1 + \Omega_{mo}^s [(a/a_o)^{-3} - 1] + \Omega_{ro}^s [(a/a_o)^{-4} - 1]} \quad (3.14)$$

with  $s = sm, smx$  for  $\Lambda$ CDM and  $\Lambda$ CDM-Nx models, respectively. Expressng  $H^{smx}$  in terms of  $sm$  quantities we have for  $\Lambda$ CDM-Nx,

$$H^{smx}(a) = H_0^{smx} \sqrt{1 + \frac{(H_0^{sm})^2}{(H_0^{smx})^2} (\Omega_{mo}^{sm} [(a/a_o)^{-3} - 1] + \Omega_{ro}^{sm} [(a/a_o)^{-4} - 1])} \quad (3.15)$$

$$= H_0^{sm} \sqrt{\frac{(H_0^{smx})^2}{(H_0^{sm})^2} + \Omega_{mo}^{sm} [(a/a_o)^{-3} - 1] + \Omega_{ro}^{sm} [(a/a_o)^{-4} - 1]}. \quad (3.16)$$

We have expressed  $H^{smx}(a)$  in terms of quantities of model  $sm$  and the ratio  $H_0^{sm}/H_0^{smx}$ . The difference in  $H^{sm}$  in  $\Lambda$ CDM and  $H^{smx}$  in  $\Lambda$ CDM-Nx due to the distinct values of  $H_0$  is manifested in the first terms in the square root in eqs.(3.14) and (3.16) ("1" in eq.(3.14) compared to  $(H_0^{smx}/H_0^{sm})^2$  in eq.(3.16)) with  $(H_0^{smx}/H_0^{sm})^2 = (H_0^R/H_0^P)^2 = (74/67)^2 = 1.22$  for our two fiducial examples.

### 3.2 Impact of $\rho_{ex}$ on the Acoustic Scale $r_s(a_*)$

We will now quantify the impact on the acoustic scale  $r_s(a_*)$  from extra relativistic energy density  $\rho_{ex}(a)$ , present before recombination, helps to conciliate the  $H_0$  tension between early and late time measurements. We assume that  $\rho_{ex}$  is present up to the scale factor  $a_c$  and than it dilutes rapidly [65] and no longer contributes to  $H$ . This rapid dilution of  $\rho_{ex}$  can be motivated by Bound Dark Energy model [61, 62] or by EDE models [21, 23]. Interestingly, the rapid dilution of  $\rho_{ex}$  besides contributing towards a solution to the  $H_0$  crisis may also leave interesting signatures in the matter power spectrum [60, 62, 64, 65, 71] which can be correlated with the  $H_0$  solution.

Let us now study the impact of  $\rho_{ex}$  on the  $H_0$  tension problem and its cosmological signatures. From eq.(3.8), we take  $H_{sm}/H_{smx} = \sqrt{1 - \Omega_{ex}}$  and for simplicity and presentation purposes we consider  $\Omega_{ex}$  constant for  $a \leq a_c$  and  $\Omega_{ex} = 0$ ,  $H_{smx} = H_{sm}$  for  $a > a_c$ . The precise impact of  $\Omega_{ex}$  and the value of  $a_c$  in the different cosmological parameters must be numerically calculated and a full implementation in a Boltzmann code Markov Chains (here we use CAMB and COSMO-MC [66–70]) is presented in section (4). Nevertheless having an approximated analytic expressions of the acoustic scale allow us to have a simple grasp of the impact of  $\rho_{ex}$  and  $a_c$  in the magnitude of  $r_s(a_*)$  and in the possible solution to the  $H_0$  crisis. The change in the acoustic scale  $r_s(a_*)$  in models  $\Lambda$ CDM ( $sm$ ) and  $\Lambda$ CDM-Nx ( $smx$ ) can be easily estimated. Let us consider the difference

$$r_s^{sm}(a_*) - r_s^{smx}(a_*) = \int_{a_i}^{a_*} \frac{c_s da}{a^2 H_{sm}} - \int_{a_i}^{a_*} \frac{c_s da}{a^2 H_{smx}} \quad (3.17)$$

$$= \int_{a_i}^{a_c} \frac{c_s da}{a^2 H_{sm}} - \int_{a_i}^{a_c} \frac{c_s da}{a^2 H_{smx}} \equiv r_s^{sm}(a_c) - r_s^{smx}(a_c) \quad (3.18)$$

where we have taken into account that  $H_{smx} = H_{sm}$  for  $a > a_c$  and the integrals from  $a_c \leq a \leq a_*$  cancel out. As long as  $H_{sm}/H_{smx} = \sqrt{1 - \Omega_{ex}}$  is constant we can simply express

$$r_s^{smx}(a_c) \equiv \int_{a_i}^{a_c} \frac{c_s da}{a^2 H_{smx}} = \int_{a_i}^{a_c} \left( \frac{H_{sm}}{H_{smx}} \right) \frac{c_s da}{a^2 H_{sm}} = \sqrt{1 - \Omega_{ex}} r_s^{sm}(a_c). \quad (3.19)$$

Clearly the amount of  $\Omega_{ex}$  determines the ratio of  $r_s^{smx}(a_*)/r_s^{sm}(a_*)$ . Now writing  $r_s^{sm}(a_*) - r_s^{smx}(a_*) = r_s^{sm}(a_*)(1 - \xi)$  with  $\xi$  given in eq.(3.6) and  $r_s^{sm}(a_c) - r_s^{smx}(a_c) = r_s^{sm}(a_c)(1 - \sqrt{1 - \Omega_{ex}})$  from eq.(3.18) we obtain  $r_s^{sm}(a_*)(1 - \xi) = r_s^{sm}(a_c)(1 - \sqrt{1 - \Omega_{ex}})$  and

$$\frac{r_s^{sm}(a_*)}{r_s^{sm}(a_c)} = \frac{1 - \sqrt{1 - \Omega_{ex}}}{1 - \xi}. \quad (3.20)$$

If we assume radiation domination, the quantity  $a^2 H$  is constant, and taking for simplicity and presentation purposes  $c_s$  also constant we get

$$\frac{r_s^{sm}(a_*)}{r_s^{sm}(a_c)} = \frac{\int_{a_i}^{a_*} \frac{da c_s}{a^2 H_{sm}}}{\int_{a_i}^{a_c} \frac{da c_s}{a^2 H_{sm}}} = \frac{a_c H_{sm}(a_c)}{a_* H_{sm}(a_*)} = \frac{a_*}{a_c} \quad (3.21)$$

and eq.(3.20) becomes

$$\left( \frac{a_*}{a_c} \right) = \frac{1 - \sqrt{1 - \Omega_{ex}}}{1 - \xi} = 52.63 (1 - \sqrt{1 - \Omega_{ex}}) \quad (3.22)$$

where we have set  $\xi = 0.981$ , our fiducial value in eq.(3.6). We obtain in eq.(3.22) a very simple analytic solution for  $a_c$  as a function of  $\Omega_{ex}$  with the constraint to have the same acoustic angle  $\theta(a_*)$  (c.f. eq.(3.1)) in  $\Lambda$ CDM-Nx with  $H_0 = 74$  as in  $\Lambda$ CDM model with  $H_0 = 67$ . We see in eq.(3.22) that larger values of  $a_c$  require smaller amount of  $\Omega_{ex}$ . We plot in fig.(1) the required value of  $N_{ex}$  and  $\Omega_{ex}$  as function of  $x = a_c/a_{eq}$  using eq.(3.22) and from the numerical calculation solving the full  $H(a)$  as given in eqs.(3.10) and (3.11). We should keep in mind that eq.(3.22) is only an approximation since we assumed radiation domination, however it gives a simple estimation of the amount of  $\Omega_{ex}$  as a function of  $a_c$  required to accommodate a consistent model with same acoustic scale with Planck data [P-18] and Riess  $H_0$  value [R-19].

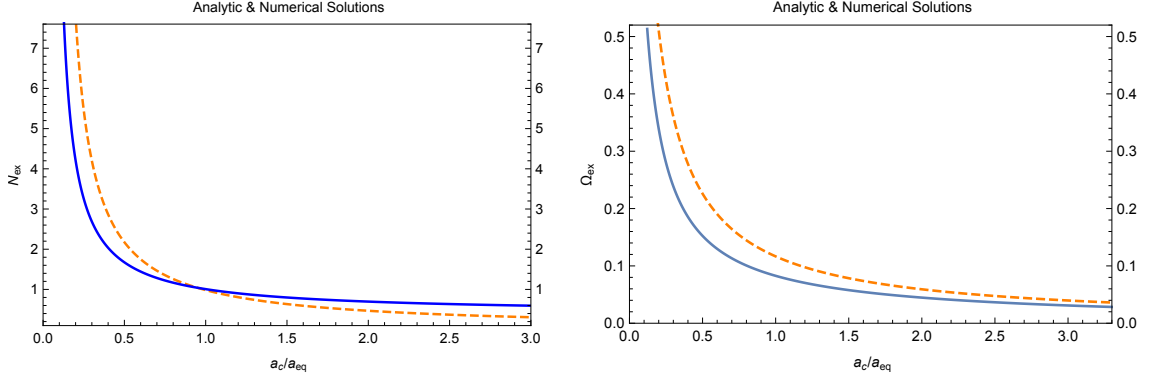


**Figure 1:** Analytic and Numerical Solutions  $N_{ex}(a_c)$  and  $\Omega_{ex}(a_c)$ . We plot  $N_{ex}$  (left panel) and  $\Omega_{ex}(a_c)$  (right panel) as a function of  $x \equiv a_c/a_{eq}$  satisfying the constraint  $r_s^{smx}(a_*)/r_s^{sm}(ad) = \xi$  (c.f. eq.(3.7)). Numerical solution (blue) and analytic solution from eq.(3.22) (dashed-orange).

### 3.3 Matter Power Spectrum and $\rho_{ex}$

We have seen in the previous section how  $\rho_{ex}$  impacts cosmological distances and contributes to reduce the  $H_0$  tension. Let us now study the effect of the rapid dilution of  $\rho_{ex}$  not only affects the evolution of density perturbations and in the matter power spectrum  $P(k, z)$  [65], [60] and [24, 32, 42, 43, 56, 57]. Interesting, an energy density  $\rho_{ex}(a)$  that dilutes rapidly at  $a = a_c$  (see section (3.2) will leave detectable imprints on the matter power spectrum which can be correlated with a possible solution to  $H_0$  tension. We can estimate the location and magnitude of this bump produced at the transition scale  $a_c$  corresponding to the mode

$$k_c \equiv a_c H_c \quad (3.23)$$

with  $H_c \equiv H(a_c)^2 = (8\pi G/3)\rho_{smx}(a_c)$  and  $\rho_{smx} = \rho_{sm} + \rho_{ex}$ . The amplitude of the bump is related to the magnitude of  $\rho_{ex}(a)$  while the width of the bump is related to how fast  $\rho_{ex}$  dilutes [65]. In radiation domination the amplitude  $\delta_m = \delta\rho_m/\rho_m$  has a logarithmic growth

$$\delta_m^{smx}(a) = \delta_{mi}^{smx} (\ln(a/a_h^{smx}) + 1/2), \quad (3.24)$$

$$\delta_m^{sm}(a) = \delta_{mi}^{sm} (\ln(a/a_h^{sm}) + 1/2) \quad (3.25)$$

where  $a_h$  corresponds to horizon crossing. Comparing this growth for the same mode  $k^{smx} = k^{sm}$  with  $k^{sm} = a_h^{sm} H^{sm}(a_h^{sm})$  and  $k^{smx} = a_h^{smx} H^{smx}(a_h^{smx})$ . Modes  $k > k_c$  cross the horizon

at  $a_h < a_c$  and we find from eq.(3.8)

$$\frac{a_h^{smx}}{a_h^{sm}} = \frac{H^{sm}}{H^{smx}} = \sqrt{1 - \Omega_{ex}}. \quad (3.26)$$

The ratio  $\Delta\delta_m = \delta_m^{smx}/\delta_m^{sm} = (\delta_{mi}^{smx}/\delta_{mi}^{sm})(\ln(a/a_h^{smx}) + 1/2)/(\ln(a/a_h^{sm}) + 1/2)$  can be expressed for  $a > a_c$  as

$$\Delta\delta_m = \frac{\delta_{mi}^{smx}}{\delta_{mi}^{sm}} \frac{[(H_+^{smx}/H_-^{smx}) \ln(a/a_c) + \ln(a_h^{sm}/a_h^{smx}) + \ln(a_c/a_h^{sm}) + \frac{1}{2}]}{\ln(a/a_c) + \ln(a_c/a_h^{sm}) + \frac{1}{2}}, \quad (3.27)$$

where  $H_+^{smx}(a_c)$  contains  $\rho_{ex}$  and  $H_-^{smx}(a_c)$  has  $\rho_{ex} = 0$ . For presentation purposes here we have consider a step function at  $a_c$  with  $\rho_{ex}(a) = 0$  for  $a < a_c$  and we have  $H_+^{smx}(a_c)/H_-^{smx}(a_c) = H^{smx}(a_c)/H^{sm} = 1/\sqrt{1 - \Omega_{ex}}$ . Eq.(3.27) is valid for modes  $k > k_c$ . entering the horizon at  $a_h < a_c$ . The increase for modes  $k > k_c$  at present time is

$$\Delta\delta_m = \frac{\delta_m^{smx}}{\delta_m^{sm}} = \frac{\delta_{mi}^{smx}}{\delta_{mi}^{sm}} \frac{H_+^{smx}}{H_-^{sm}} = \frac{\delta_{mi}^{smx}}{\delta_{mi}^{sm}} \frac{1}{\sqrt{1 - \Omega_{ex}}} \quad (3.28)$$

where we assumed for  $a_o \gg a_c$ . On the other hand modes  $k < k_c$  do not undergo the transition and are not boosted by the rapid dilution of  $\rho_{ex}$ . The final result in the matter power spectrum is the generation of a bump in the ratio  $P_{smx}/P_{sm}$  at scales of the order of  $k_c$ .

To conclude, we have seen in our toy model that an extra relativistic energy density  $\rho_{ex}$  may alleviate the tension in the  $H_0$  measurements and at the same time leave detectable signals in the matter power spectrum allowing for a verification of the proposal.

## 4 Cosmological Results and MCMC implementation

We consider here two models, the first one is simple the standard  $\Lambda$ CDM model while our second model corresponds to an extension to  $\Lambda$ CDM, where we add extra relativistic energy density  $\rho_{ex}(a) \propto 1/a^3$  present only at early times for a scale factor  $a$  smaller than  $a_c$ , corresponding to the transition scale factor, and the extra energy density dilutes as  $\rho_{ex} \propto a^{-6}$  for  $a \gg a_c$  and becomes therefore rapidly negligible. We refer to this later model as  $\Lambda$ CDM-Nx and is motivated by Bound Dark Energy (BDE) model [61, 62] and EDE models [41–44].

With this rapid dilution we avoid a step function transition at  $a_c$  in the evolution of  $\rho_{ex}(a)$ . Clearly  $\rho_{ex}$  dilutes faster than radiation for  $a > a_c$  and its contribution becomes rapidly subdominant. The energy density  $\rho_{ex}$  can also be parametrized by the number of extra relativistic degrees of freedom  $N_{ex}$ , defined in terms of the the neutrino temperature  $T_\nu$  as  $\rho_{ex} = (\pi^2/30)N_{ex}T_\nu^4$ . We implement the  $\Lambda$ CDM-Nx model in the Boltzmann code CAMB [66–70]) and make a full COSMO-MC (Markov Chains) analysis for  $\Lambda$ CDM and  $\Lambda$ CDM-Nx for several data sets and we present the results and conclusions in section (4.1).

Since our main interest here is to study the tension between the inferred value of  $H_0$  from early CMB physics and late time local measurements of  $H_0$  we use the CMB (TT, TE, EE+lowE) data set from Planck 2018 [P1-18] [9] and the recent measurements from SH0S  $H_0^R = (74.03 \pm 1.42)$  at 68% confidence level by Riess et al [R19] [1]. We run MCMC for both models,  $\Lambda$ CDM and  $\Lambda$ CDM-Nx, and compare the posterior probabilities and we assess the viability to alleviate the  $H_0$  tension between CMB from Planck [P18] and local  $H_0$  measurements [R19]. We decided not to use BAO measurements, keeping in mind that

BAO is consistent with high and low values of  $H_0$  and it is in the context of  $\Lambda$ CDM that BAO measurements hint for a lower value of  $H_0$  [59]. Besides BAO analysis is strongly impacted by the late time dynamics of dark energy at low redshifts  $z < 5$ . Changes from a dynamical the dark energy are beyond the scope of this work since we want to concentrate on the tension between CMB and local  $H_0$  measurements.

For our analysis we consider besides the recent measurement  $H_0^R = 74.03 \pm \sigma_H$  with  $\sigma_H = 1.42$  at 68% confidence level (we will quote all values of  $H_0$  and  $\sigma_H$  in units of  $\text{km s}^{-1} \text{Mpc}^{-1}$ ) two forecasting values of  $\sigma_H$  and we take these forecasting values as  $\sigma_H = 1$  and  $\sigma_H = 0.5$ . With these two forecasting values of  $\sigma_H$  we impose a "tighter observational" constraint on  $H_0$  from local measurements to study the impact on the posterior probabilities of  $H_0$  and other relevant cosmological parameters in  $\Lambda$ CDM and  $\Lambda$ CDM-Nx models, and we assess the price we have to pay on the "Goodness of Fit" of CMB  $\chi_{cmb}^2$  for these two forecasting values of  $H_0$ . Notice however that these forecasting values,  $\sigma_H = 1$  and  $\sigma_H = 0.5$ , are of the same order as the average value obtained in the review L.Verde, A. Riess and T.True [14] with an average value of local measurements of  $H_0 = (73.03 \pm 0.8) \text{ km s}^{-1} \text{Mpc}^{-1}$ .

We first consider the MCMC results using CMB data [P-18] and  $H_0 = (74.02 \pm \sigma_H)$  with  $\sigma_H = 1.42$  [R-19]. We show the best fit and the marginalized values at 68% confidence level for  $\Lambda$ CDM-Nx and  $\Lambda$ CDM for different cosmological parameters in table 1. For completeness we also include  $\Lambda$ CDM without Riess  $H_0$  data set (we refer to this case as "No-Riess"). Notice that the value of  $H_0$  in table 1 is a slight increase from  $H_0 = (67.99 \pm 0.45)$  in  $\Lambda$ CDM without Riess data [R-19] to  $H_0 = (68.54 \pm 0.43)$  for  $\Lambda$ CDM and a value of  $H_0 = (68.70 \pm 0.45)$  in  $\Lambda$ CDM-Nx considering in these last two cases Riess data [R-19]. The values of  $H_0$  correspond to a mild increase of 0.81% and 1.04%, in the value of  $H_0$  for  $\Lambda$ CDM and  $\Lambda$ CDM-Nx, respectively. These values of  $H_0$  are still in disagreement with local measurements [R-19]. The model  $\Lambda$ CDM-Nx contains extra radiation  $\Omega_{ex}(a_c) = 0.063 (+0.146, -0.021)$  with  $N_{ex} = 0.0903 (+0.28, -0.79)$  at 68% confidence level.

We follow up our analysis by considering  $H_0^R = (74.03 \pm \sigma_H)$  with the two forecasting values  $\sigma_H = 1$  and  $\sigma_H = 0.5$ . With these forecasting values on  $\sigma_H$  we impose a tighter constraint on the value of  $H_0$  and this allows to assess the impact on the posterior probabilities of the cosmological parameters as well as the Goodness fit for CMB  $\chi_{cmb}^2$ . We implemented these forecasting  $\sigma_H = 1$  and  $\sigma_H = 0.5$  in the MCMC analysis for  $\Lambda$ CDM and  $\Lambda$ CDM-Nx models. We show the best fit values and posterior probabilities at 68% c.l. in table 2 for  $\Lambda$ CDM and in table 3 for  $\Lambda$ CDM-Nx. We find for  $\Lambda$ CDM model with the forecasting  $\sigma_H = 1$  a value of  $H_0 = 69.04 \pm 0.41$  (68% c.l.) and a best fit value  $H_0 = 69.05$ , while for  $\sigma_H = 0.5$  we find  $H_0 = 70.79 \pm 0.36$  (68% c.l.) and  $H_0 = 70.79$  for the best fit. While in  $\Lambda$ CDM-Nx model we obtain for  $\sigma_H = 1$  a value  $H_0 = 69.19 \pm 0.44$ , with a best fit  $H_0 = 69.23$  and for  $\sigma_H = 0.5$  we get  $H_0 = 72.99 \pm 0.47$  and a best fit  $H_0 = 72.83$ , respectively. We notice that the impact of a reduced  $\sigma_H = 0.5$  substantially increases the value of  $H_0$  in  $\Lambda$ CDM-Nx but not in  $\Lambda$ CDM model. This is no surprise and is a consequence of the contribution of the extra relativistic energy density  $\rho_{ex}$  in  $\Lambda$ CDM-Nx.

We present the best fit values and marginalized 68% and 95% parameters constraint contours for different cosmological parameters for  $\Lambda$ CDM in fig.(2) and for  $\Lambda$ CDM-Nx in fig.(3). We find useful to include in a single graph the marginalized 68% and 95% parameters constraint contours  $\Lambda$ CDM,  $\sigma_H = 1.42$ ,  $\sigma_H = 0.5$  and No-Riess supplemented with  $\Lambda$ CDM-Nx with  $\sigma_H = 0.5$  in fig.(4). This last graph allows for a convenient comparison of the posteriors between  $\Lambda$ CDM models and  $\Lambda$ CDM-Nx with  $\sigma_H = 0.5$  and the impact on the value of  $H_0$  and other parameters.

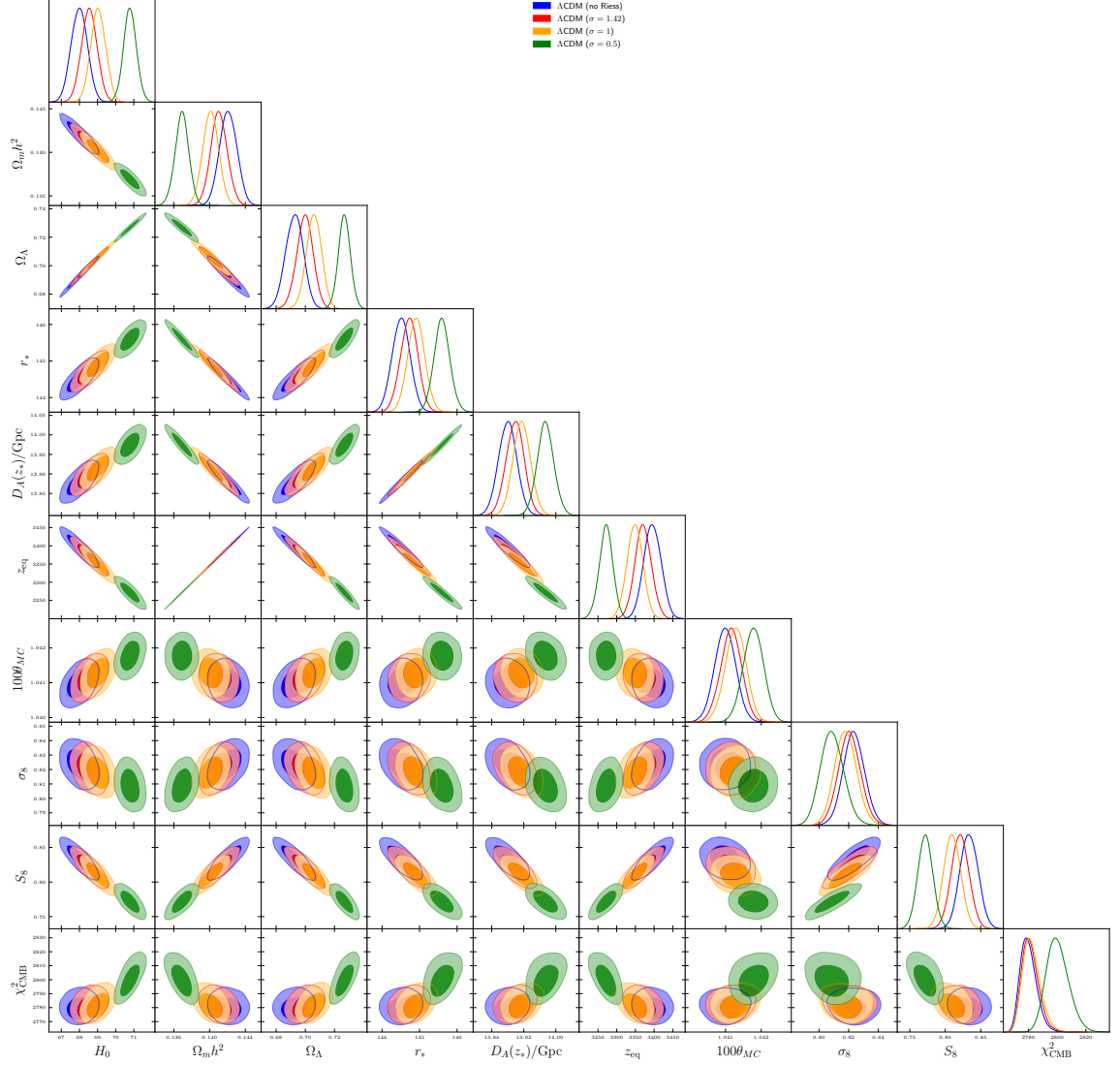


**Figure 2:** We show the marginalized 68% and 95% parameters constraint contours for  $\Lambda$ CDM using Planck-2018 TT,TE,EE,lowE [P18] and  $H_0 = (74.03 \pm \sigma_H) \text{ km s}^{-1} \text{ Mpc}^{-1}$  with  $\sigma_H = 1.42$  [R-19], the forecasting values  $\sigma_H = 1, 0.5$  and  $\Lambda$ CDM without Riess data set.

The best fit values for  $N_{ex}$ ,  $\Omega_{ex}(a_c)$  and the transition scale factor  $a_c$  for the three  $\Lambda$ CDM-Nx cases are:  $N_{ex} = 0.09$ ,  $\Omega_{ex}(a_c) = 0.0035$  and  $a_c = (7.1 \times 10^{-4})$  for  $H_0$  with  $\sigma_H = 1.42$ ,  $N_{ex} = 0.07$ ,  $\Omega_{ex}(a_c) = 0.0062$  and  $a_c = (1.5 \times 10^{-4})$  for  $H_0$  with  $\sigma_H = 1$  and  $N_{ex} = 0.61$ ,  $\Omega_{ex}(a_c) = 0.006$  and  $a_c = (3.48 \times 10^{-3})$  for  $H_0$  with  $\sigma_H = 0.5$ . Notice that the amount of  $\Omega_{ex}(a_c)$  remains of the same order of magintude in all three  $\Lambda$ CDM-Nx cases while we get an increase of  $N_{ex}$  and  $a_c$  by factor of about 10 times larger in  $\Lambda$ CDM-Nx with  $\sigma_H = 0.5$  compared to  $\Lambda$ CDM-Nx with  $\sigma_H = 1.42$  or  $\sigma_H = 1$ .

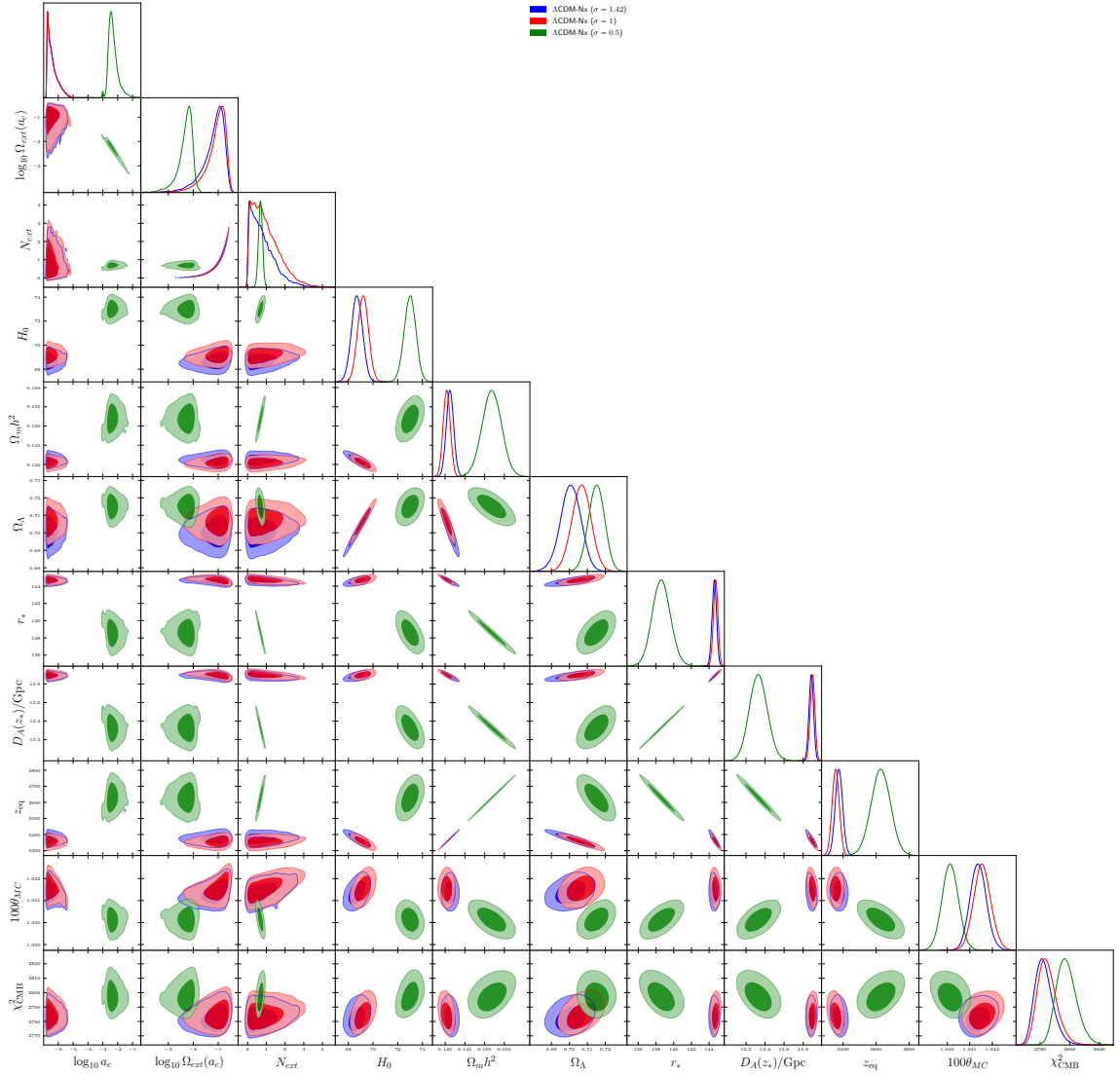


**Figure 3:** We show the marginalized 68% and 95% parameters constraint contours for  $\Lambda$ CDM-Nx using Planck-2018 TT,TE,EE,lowE and  $H_0 = (74.03 \pm \sigma_H) \text{ km s}^{-1} \text{ Mpc}^{-1}$  with  $\sigma_H = 1.42$  [R-19] and the forecasting values  $\sigma_H = 1, 0.5$ .

#### 4.1 Analysis

Let us now compare and analyze the results of the MCMC results in  $\Lambda$ CDM and  $\Lambda$ CDM-Nx models given in tables 1, 2 and 3. Besides these three tables with the best fit and sampling values for different cosmological parameters in  $\Lambda$ CDM and  $\Lambda$ CDM-Nx models and the corresponding figures at 68% and 95% marginalized parameters constraint contours in fig.2 for  $\Lambda$ CDM, fig.3 for  $\Lambda$ CDM-Nx, and the mixed fig. 4, we find useful to analyze the difference between these cases by determining the relative difference and the percentage difference for some relevant parameters shown in tables 5 and 6, respectively.

We show in table 4 the discrepancy between the value of  $H_0 = 74.03 \pm \sigma_H$ , for the three different values of  $\sigma_H$  (i.e.  $\sigma_H = 1.42, 1, 0.5$ ), and the posterior probability of  $H_0 \pm \sigma_s$  with

Model Parameter	$\Lambda$ CDM-Nx Best Fit	$H_0 = (74.03 \pm 1.42)$ Sampling	$\Lambda$ CDM Best Fit	$H_0 = 74.03 \pm 1.42$ Sampling	$\Lambda$ CDM Best Fit	$H_0$ No-Riess Sampling
$a_c$	0.00071	$0.407^{+0.105}_{-0.241} \times 10^{-6}$	—	—	—	—
$\Omega_{ex}(a_c)$	0.00353	$0.063^{+0.146}_{-0.021}$	—	—	—	—
$N_{ex}$	0.09034	$0.81^{+0.22}_{-0.79}$	—	—	—	—
$H_0$	69.14	$68.70 \pm 0.45$	68.557	$68.54 \pm 0.43$	67.961	$67.99 \pm 0.45$
$\Omega_\Lambda$	0.702	$0.7007 \pm 0.0057$	0.700	$0.6997 \pm 0.0056$	0.692	$0.6925 \pm 0.0060$
$\Omega_m$	0.298	$0.2993 \pm 0.0057$	0.300	$0.3003 \pm 0.0056$	0.308	$0.3075 \pm 0.0060$
$\Omega_m h^2$	0.142	$0.14123 \pm 0.00093$	0.141	$0.14106 \pm 0.00092$	0.142	$0.14209 \pm 0.00096$
$\Omega_b h^2$	0.022	$0.02257 \pm 0.00014$	0.022	$0.02248 \pm 0.00013$	0.022	$0.02237 \pm 0.00013$
$z_{eq}$	3398.84	$3375 \pm 22$	3370.15	$3371 \pm 22$	3397.99	$3396 \pm 23$
$\ln(10^{10} A_s)$	3.048	$3.049 \pm 0.017$	3.047	$3.046 \pm 0.017$	3.044	$3.045 \pm 0.016$
$n_s$	0.973	$0.9722^{+0.0043}_{-0.0049}$	0.970	$0.9683 \pm 0.0037$	0.966	$0.9655 \pm 0.0038$
$\sigma_8$	0.826	$0.8237 \pm 0.0079$	0.821	$0.8206 \pm 0.0075$	0.824	$0.8235 \pm 0.0072$
$S_8$	0.823	$0.823 \pm 0.013$	0.821	$0.821 \pm 0.012$	0.835	$0.834 \pm 0.013$
$z_{drag}$	1089.81	$1060.63^{+0.38}_{-0.56}$	1060.12	$1060.09 \pm 0.28$	1059.93	$1059.92 \pm 0.28$
$r_{drag}$	146.60	$101.11 \pm 0.76$	147.35	$147.35 \pm 0.24$	147.14	$147.17 \pm 0.24$
$z_*$	1060.24	$1089.95^{+0.26}_{-0.35}$	1089.63	$1089.65 \pm 0.21$	1089.88	$1089.88 \pm 0.22$
$r_*$	143.98	$144.58 \pm 0.25$	144.72	$144.72 \pm 0.23$	144.48	$144.51 \pm 0.24$
$D_A(r_*)/\text{Gpc}$	13.829	$13.885 \pm 0.024$	13.899	$13.898 \pm 0.022$	13.877	$13.880 \pm 0.023$
$100\theta(z_*)$	1.0410	$1.04137 \pm 0.00036$	1.0411	$1.04115 \pm 0.00029$	1.0410	$1.04099 \pm 0.00029$
$\chi^2_{H_0}$	11.84	$14.2 \pm 2.4$	14.854	$15.0 \pm 2.4$	—	—
$\chi^2_{CMB}$	2766.24	$2782.6 \pm 6.1$	2765.69	$2781.3 \pm 5.8$	2764.35	$2780.0 \pm 5.7$

**Table 1:** We show the best fit, marginalized and 68% confidence limits on cosmological parameters for  $\Lambda$ CDM-Nx and  $\Lambda$ CDM with Planck-2018 TT,TE,EE-lowE and local  $H_0$  R-19 measurements and  $\Lambda$ CDM without R-19 (i.e. "No-Riess").

Model Parameter	$\Lambda$ CDM Best Fit	$H_0 = 74.03 \pm 1$ Sampling	$\Lambda$ CDM Best Fit	$H_0 = 74.03 \pm 0.5$ Sampling
$H_0$	69.050	$69.04 \pm 0.41$	70.789	$70.79 \pm 0.36$
$\Omega_\Lambda$	0.706	$0.7059 \pm 0.0052$	0.727	$0.7268 \pm 0.0041$
$\Omega_m$	0.294	$0.2941 \pm 0.0052$	0.273	$0.2732 \pm 0.0041$
$\Omega_m h^2$	0.140	$0.14013 \pm 0.00089$	0.137	$0.13690 \pm 0.00077$
$\Omega_b h^2$	0.023	$0.02258 \pm 0.00013$	0.023	$0.02291 \pm 0.00013$
$z_{eq}$	3349.60	$3349 \pm 21$	3272.72	$3272 \pm 18$
$\ln(10^{10} A_s)$	3.046	$3.046 \pm 0.017$	3.049	$3.051^{+0.017}_{-0.019}$
$n_s$	0.972	$0.9712 \pm 0.0036$	0.981	$0.9805 \pm 0.0036$
$\sigma_8$	0.818	$0.8180 \pm 0.0074$	0.808	$0.8089^{+0.0072}_{-0.0082}$
$S_8$	0.810	$0.810 \pm 0.012$	0.772	$0.772 \pm 0.011$
$z_{drag}$	1060.31	$1060.24 \pm 0.27$	1060.77	$1060.73 \pm 0.28$
$r_{drag}$	147.48	$147.51 \pm 0.24$	148.08	$148.11 \pm 0.23$
$z_*$	1089.41	$1089.44 \pm 0.20$	1088.72	$1088.74 \pm 0.18$
$r_*$	144.89	$144.91 \pm 0.23$	145.58	$145.60 \pm 0.21$
$D_A(r_*)/\text{Gpc}$	13.913	$13.915 \pm 0.022$	13.973	$13.974 \pm 0.021$
$100\theta(z_*)$	1.0413	$1.04128 \pm 0.00029$	1.0418	$1.04178 \pm 0.00028$
$\chi^2_{H_0}$	24.797	$25 \pm 4$	42.027	$42 \pm 9$
$\chi^2_{CMB}$	2766.43	$2782.1 \pm 6.2$	2784.45	$2800.3 \pm 7.8$

**Table 2:** We show the best fit, marginalized and 68% confidence limits for  $\Lambda$ CDM with Planck-2018 TT,TE,EE-lowE and  $H_0 = 74.02 \pm \sigma_H$  with forecasting value  $\sigma_H = 1$  and  $\sigma_H = 0.5$

$\sigma_s$  the 68% confidence level for  $\Lambda$ CDM and  $\Lambda$ CDM-Nx from the MCMC. The central value of  $H_0$  of the samplings increases with decreasing  $\sigma_H$ , while the amplitude of  $\sigma_s$  remains nearly constant in all 6 cases ( $\sigma_s \sim 0.42$ ). The quantity  $\Delta H_0 \equiv (74.03 - H_0)$  corresponds to the distance between the central value  $H_0 = 74.03$  from Riess [R-19] and the central value  $H_0$  from each of the samplings and we define  $\sigma_T \equiv \sigma_H + \sigma_s$  for each case. Not surprisingly for smaller values of  $\sigma_H$  we obtain a larger  $H_0$  and a decrease in  $\Delta H_0/\sigma_T$  in  $\Lambda$ CDM and  $\Lambda$ CDM-Nx models. However, even though the value of  $H_0$  increases so does  $\chi^2_{H_0}$  in all cases but for  $\Lambda$ CDM-Nx with  $\sigma_H = 0.5$ . We obtain in  $\Lambda$ CDM model  $\chi^2_{H_0} = 15 \pm 2.4$  for  $\sigma_H = 1.42$ ,  $\chi^2_{H_0} = 25 \pm 4$  for  $\sigma_H = 1$  and  $\chi^2_{H_0} = 42 \pm 9$  for  $\sigma_H = 0.5$ , while in  $\Lambda$ CDM-Nx we have

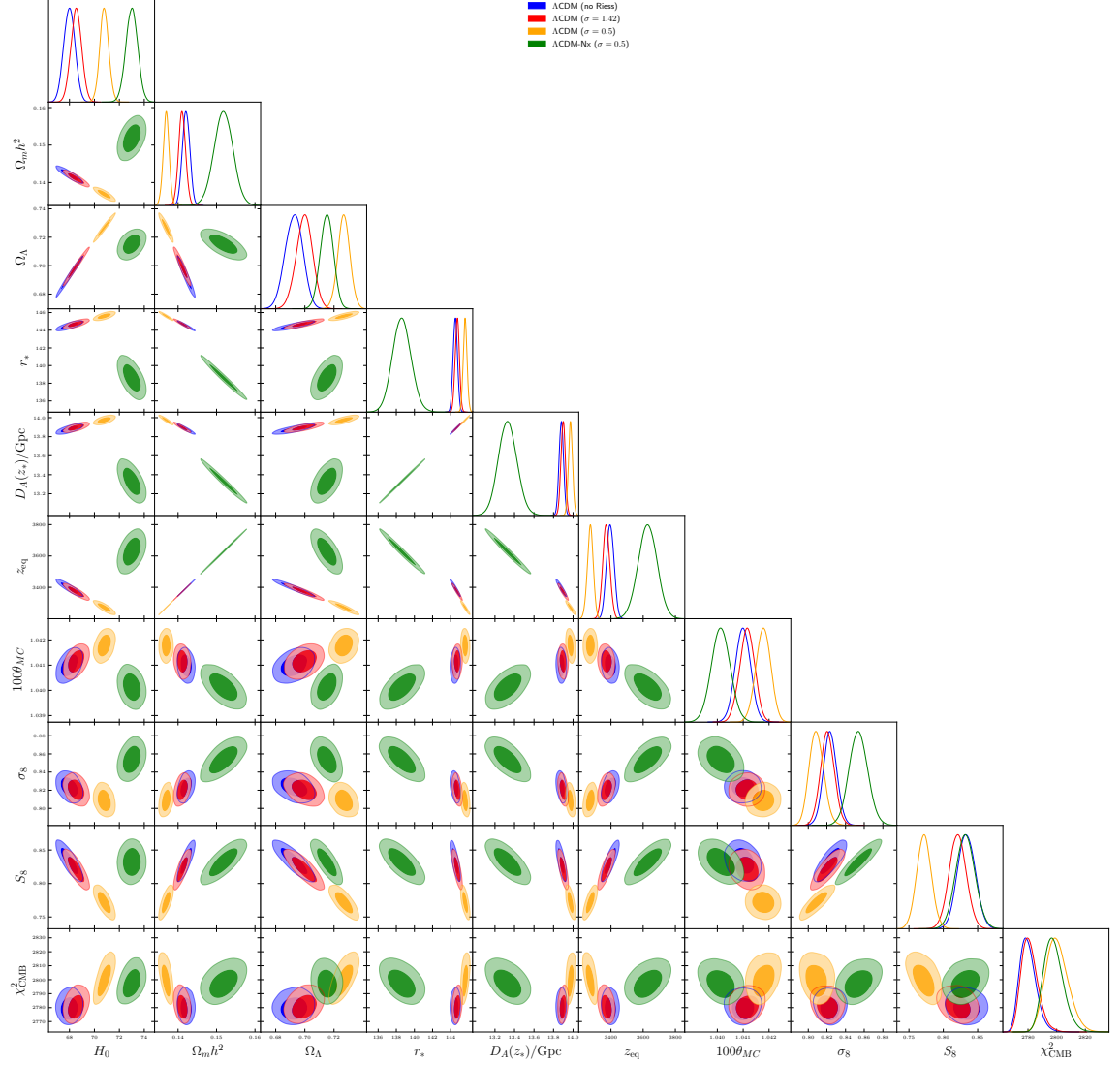


**Figure 4:** We show the marginalized 68% and 95% parameters constraint contours using Planck 2018 TT,TE,EE,lowE and  $H_0 = (74.03 \pm 0.5) \text{ km s}^{-1} \text{ Mpc}^{-1}$  for  $\Lambda\text{CDM-Nx}$  and  $H_0 = (74.03 \pm \sigma_H) \text{ km s}^{-1} \text{ Mpc}^{-1}$  with  $\sigma_H = 1.42$  [R-19] and the forecasting values  $\sigma_H = 0.5$  and No-Riess for  $\Lambda\text{CDM}$  models.

$\chi^2_{H_0} = 14.2 \pm 2.4$  for  $\sigma_H = 1.42$  and  $\chi^2_{H_0} = 24 \pm 4$  for  $\sigma_H = 1$  while we have significant reduction in  $\sigma_H = 0.5$  model obtaining  $\chi^2_{H_0} = 5.2 \pm 4.2$ . Notice that the difference in  $\chi^2_{H_0}$  between  $\Lambda\text{CDM}$  and  $\Lambda\text{CDM-Nx}$  is small for  $\sigma_H = 1.42$  and  $\sigma_H = 1$  however the impact from the forecasting value  $\sigma_H = 0.5$  in  $\Lambda\text{CDM-Nx}$  has a significant reduction in  $\chi^2_{H_0}$  from  $\chi^2_{H_0} = 42 \pm 9$  in  $\Lambda\text{CDM}$  to  $\chi^2_{H_0} = 5.2 \pm 4.2$  in  $\Lambda\text{CDM-Nx}$ . We remark that only  $\Lambda\text{CDM-Nx}$  with  $\sigma_H = 0.5$  has an  $\Delta H_0/\sigma_T$  smaller than one, clearly showing the impact of the reduced  $\sigma_H$ .

In order to assess the impact of the reduced forecasting value  $\sigma_H = 0.5$  in  $\Lambda\text{CDM-Nx}$  on different cosmological parameters we compare the results from  $\Lambda\text{CDM-Nx}$  with  $\sigma_H = 0.5$  and  $\Lambda\text{CDM}$  with  $\sigma_H = 1.42, \sigma_H = 0.5$  and No-Riess in table 5 and we determine the relative

Model Parameter	$\Lambda$ CDM-Nx Best Fit	$H_0 = 74.03 \pm 1$ Sampling	$\Lambda$ CDM-Nx Best Fit	$H_0 = 74.03 \pm 0.5$ Sampling
$a_c$	0.00015	$0.407^{+0.105}_{-0.245} \times 10^{-6}$	0.00348	$4.898^{+2.247}_{-2.710} \times 10^{-3}$
$\Omega_{ex}(a_c)$	0.00623	$0.079^{+0.161}_{-0.023}$	0.00603	$4.786^{+5.447}_{-1.319} \times 10^{-3}$
$N_{ex}$	0.07059	$0.99^{+0.28}_{-0.95}$	0.60916	$0.69 \pm 0.10$
$H_0$	69.23	$69.19 \pm 0.44$	72.83	$72.99 \pm 0.47$
$\Omega_\Lambda$	0.705	$0.7067 \pm 0.0053$	0.718	$0.7151 \pm 0.0045$
$\Omega_m$	0.2949	$0.2933 \pm 0.0053$	0.2825	$0.2849 \pm 0.0045$
$\Omega_m h^2$	0.1413	$0.14039 \pm 0.00090$	0.1499	$0.1518 \pm 0.0024$
$\Omega_b h^2$	0.0227	$0.02267 \pm 0.00015$	0.0230	$0.02300 \pm 0.00012$
$z_{eq}$	3377.26	$3355 \pm 22$	3581.23	$3628 \pm 59$
$\ln(10^{10} A_s)$	3.0502	$3.051 \pm 0.017$	3.0699	$3.076^{+0.016}_{-0.018}$
$n_s$	0.9776	$0.9753^{+0.0046}_{-0.0052}$	0.9911	$0.9917 \pm 0.0040$
$\sigma_8$	0.8258	$0.8220 \pm 0.0080$	0.8472	$0.854 \pm 0.010$
$S_8$	0.8187	$0.813 \pm 0.012$	0.8221	$0.832 \pm 0.014$
$z_{drag}$	1060.58	$1060.87^{+0.43}_{-0.61}$	1062.30	$1062.51 \pm 0.38$
$r_{drag}$	146.92	$147.31 \pm 0.28$	141.80	$141.0 \pm 1.0$
$z_*$	1089.45	$1089.83^{+0.28}_{-0.36}$	1090.31	$1090.53 \pm 0.32$
$r_*$	144.36	$144.74 \pm 0.26$	139.40	$138.6 \pm 1.0$
$D_A(r_*)$	13.860	$13.899 \pm 0.024$	13.404	$13.330 \pm 0.095$
$100\theta(z_*)$	1.0414	$1.04155 \pm 0.00038$	1.0403	$1.04013 \pm 0.00036$
$\chi^2_{H0}$	23.031	$24 \pm 4$	5.71714	$5.2 \pm 4.2$
$\chi^2_{CMB}$	2767.06	$2784.9 \pm 6.4$	2779.81	$2797.9 \pm 6.9$

**Table 3:** We show the best fit, marginalized and 68% confidence limits for  $\Lambda$ CDM-Nx with Planck-2018 TT,TE,EE-lowE and  $H_0 = 74.02 \pm \sigma_H$  with forecasting value  $\sigma_H = 1$  and  $\sigma_H = 0.5$

Model $H_0 = 74.03 \pm \sigma_H$	$\Lambda$ CDM $\sigma_H = 1.42$	$\Lambda$ CDM $\sigma_H = 1$	$\Lambda$ CDM $\sigma_H = 0.5$	$\Lambda$ CDM-Nx $\sigma_H = 1.42$	$\Lambda$ CDM-Nx $\sigma_H = 1$	$\Lambda$ CDM-Nx $\sigma_H = 0.5$
$H_0 \pm \sigma_s$	$68.54 \pm 0.43$	$69.04 \pm 0.41$	$70.79 \pm 0.36$	$68.70 \pm 0.45$	$69.19 \pm 0.44$	$72.99 \pm 0.47$
$\sigma_T = \sigma_H + \sigma_s$	$1.42 \pm 0.43$	$1 \pm 0.41$	$0.5 \pm 0.36$	$1.42 \pm 0.45$	$1 \pm 0.44$	$0.5 \pm 0.36$
$\Delta H_0 / \sigma_T$	2.968	2.697	1.820	2.850	2.602	0.550
$\chi^2_{H_0}$	$15.0 \pm 2.4$	$25 \pm 4$	$42 \pm 9$	$14.2 \pm 2.4$	$24 \pm 4$	$5.2 \pm 4.2$

**Table 4:** We show the central value  $H_0$  and the 68% confidence level ( $\sigma_s$ ) of the MCMC samplings using Planck-2018 and  $H_0 = 74.02 \pm \sigma_H$  with different values of  $\sigma_H$  in  $\Lambda$ CDM and  $\Lambda$ CDM-Nx models. The value  $\sigma_H = 1.42$  corresponds to local measurements (R-19) while  $\sigma_H = 1$  and  $\sigma_H = 0.5$  the two forecasting values of local  $H_0$  measurements, while  $\sigma_s$  corresponds to the sampling margin at 68% confidence level. We see that the central value of  $H_0$  increases with decreasing  $\sigma_H$  while the distance in  $\Delta H_0 / \sigma_T$  becomes smaller with  $\sigma_T = \sigma_H + \sigma_s$ . The reduction is far more prominent in  $\Lambda$ CDM-Nx than in  $\Lambda$ CDM. Finally we show in the last two lines the  $\chi^2$  for  $H_0$  and CMB sampling with the different data sets.

Model	$100\theta(z_*)$	$D_A(r_*)$	$r_*$	$H_0$	$\Omega_m h^2$	$z_{eq}$	$\sigma_8$	$S_8$	$\chi^2_{H_0}$	$\chi^2_{cmb}$
$\Lambda$ CDM-Nx $\sigma_H = 0.5$	1.04027	13.404	139.40	72.83	0.1499	3581.23	0.847	0.822	5.72	2779.81
$\Lambda$ CDM $\sigma_H = 0.5$	0.146	4.239	4.429	-2.809	-8.612	-8.615	-4.591	-6.156	635.111	0.167
$\Lambda$ CDM $\sigma_H = 1.42$	0.082	3.688	3.815	-5.873	-5.892	-5.894	-3.062	-0.094	159.815	-0.508
$\Lambda$ CDM No-Riess	0.068	3.525	3.639	-6.691	-5.115	-5.117	-2.748	1.524	—	-0.556

**Table 5:** We show in the 2nd line the best fit values for  $\Lambda$ CDM-Nx with  $H_0 = (1.42 \pm 0.5) \text{ km s}^{-1} \text{ Mpc}^{-1}$  and we present the relative percent difference  $\Delta_{RPD}P \equiv 100 (P_\Lambda - P_{Nx}) / P_{Nx}$  for different parameters between  $\Lambda$ CDM-Nx (with  $\sigma_H = 0.5$ ) and  $\Lambda$ CDM models for different values of  $\sigma_H = 0.5, 1.42$  and No-Riess.

Best Fit Models $H_0 = 74.03 \pm \sigma_H$	$\Lambda$ CDM-Nx $\sigma_H = 0.5$	$\Lambda$ CDM-Nx $\sigma_H = 1.42$	$\Lambda$ CDM-Nx $\sigma_H = 1$	$\Lambda$ CDM No-Riess	$\Lambda$ CDM $\sigma_H = 1.42$	$\Lambda$ CDM $\sigma_H = 1$	$\Lambda$ CDM $\sigma_H = 0.5$
$H_0$ $(H_R - H_0)/1.42$	72.83 0.83	69.14 3.43	69.23 3.37	67.96 4.27	68.56 3.85	69.05 3.50	70.79 2.28
Parameter	$\Lambda$ CDM-Nx	% Diff.	% Diff.	% Diff.	% Diff.	% Diff.	% Diff.
$H_0$	72.83	1.30	1.27	1.73	1.51	1.33	0.71
$\Omega_\Lambda$	0.72	0.53	0.43	0.90	0.62	0.40	-0.32
$\Omega_m$	0.28	-1.29	-1.07	-2.15	-1.51	-1.00	0.83
$\Omega_m h^2$	0.15	1.31	1.47	1.31	-1.51	1.67	2.25
$\Omega_b h^2$	0.02	0.55	0.33	0.66	0.54	0.41	0.07
$z_{eq}$	3581.23	1.31	1.47	1.31	1.52	1.67	2.25
$\sigma_8$	0.85	0.63	0.64	0.70	0.78	0.87	1.17
$S_8$	0.82	-0.01	0.10	-0.38	0.02	0.37	1.59
$z_{drag}$	1062.30	-0.64	0.04	0.06	0.05	0.05	0.04
$r_{drag}$	141.80	-0.83	-0.89	-0.92	-0.96	-0.98	-1.08
$z_*$	1090.31	0.70	0.02	0.01	0.02	0.02	0.04
$r_*$	139.40	-0.81	-0.87	-0.89	-0.94	-0.96	-1.08
$D_A(r_*)$	13.40	-0.78	-0.84	-0.87	-0.91	-0.93	-1.04
$100 \theta(z_*)$	1.04027	-0.02	-0.03	-0.02	-0.02	-0.02	-0.04
$\chi^2_{H_0}$	5.72	-17.44	-30.11	—	-22.21	-31.26	-38.03
$\chi^2_{cmb}$	2779.81	0.122	0.11	0.14	0.13	0.12	-0.04

**Table 6:** We show the percentage difference  $\Delta P \equiv 100(P_{Nx} - P_\Lambda)/[(P_{Nx} + P_\Lambda)/2]$  of different parameters between  $\Lambda$ CDM-Nx (with  $\sigma_H = 0.5$ ) and the different  $\Lambda$ CDM-Nx and  $\Lambda$ CDM cases with  $H_0 = 74.03 \pm \sigma_H$  and No-Riess.

percent difference between  $\Lambda$ CDM-Nx with  $\sigma_H = 0.5$  with  $\Lambda$ CDM for several parameters and we show in table 6 the percentage difference of several parameters between  $\Lambda$ CDM-Nx with  $\sigma_H = 0.5$  and  $\Lambda$ CDM-Nx with  $\sigma_H = 1$  and  $\sigma_H = 1.42$  as well as  $\Lambda$ CDM with  $\sigma_H = 0.5, \sigma_H = 0.5 = 1, \sigma_H = 1.42$  and No-Riess.

In table 5 we present the relative percent difference (RPD)  $\Delta_{RPD}P \equiv 100(P_\Lambda - P_{Nx})/P_{Nx}$  between  $\Lambda$ CDM-Nx (with  $\sigma_H = 0.5$ ) and  $\Lambda$ CDM models (with  $\sigma_H = 0.5, \sigma_H = 0.142$  and No-Riess). Not surprisingly the change in  $\theta$  is small ( $\Delta_{RPD}\theta < 0.15\%$ ) while we get a decrease in  $D_A(r_*)$  and  $r(r_*)$  of the same order ( $\Delta_{RPD} \sim 4\%$  for both quantities), while we have a  $\Delta_{RPD}H_0$  of 6.7%, 5.9% and 2.8% with respect to  $\Lambda$ CDM (No-Riess,  $\sigma_H = 1.42$  and  $\sigma_H = 0.5$ , respectively). Furthermore, notice that  $\Lambda$ CDM-Nx ( $\sigma_H = 0.5$ ) has a significant reduction in  $\chi^2_{H_0}$  compared to  $\Lambda$ CDM corresponding to a  $\Delta_{RPD}\chi^2_{H_0}$  of 635% vs  $\Lambda$ CDM ( $\sigma_H = 0.5$ ) and 159% vs  $\Lambda$ CDM ( $\sigma_H = 1.42$ ). On the other hand,  $\Lambda$ CDM-Nx ( $\sigma_H = 0.5$ ) increases  $\chi^2_{cmb}$  by 0.556% against  $\Lambda$ CDM (No-Riess), 0.508% vs  $\Lambda$ CDM ( $\sigma_H = 1.42$ ) while it reduces  $\chi^2_{cmb}$  by 0.167% vs  $\Lambda$ CDM ( $\sigma_H = 0.5$ ).

In table 6 we show in the two first lines the value of  $H_0$  and the distance between obtained Best Fit values of  $H_0$  for the different cases and the central value of  $H_0 = 74.03$  divided by the quoted observational error  $\sigma_H = 1.42$  in [R19]. Notice that only  $\Lambda$ CDM-Nx (with  $\sigma_H = 0.5$ ) with a value of  $H_0 = 72.83$  has a value below one  $\sigma_H = 1.42$  while in all other cases the distance is above two  $\sigma_H = 1.42$ . We also show in table 6 the percentage difference  $\Delta P \equiv 100(P_{Nx} - P_\Lambda)/[(P_{Nx} + P_\Lambda)/2]$  between  $\Lambda$ CDM-Nx ( $\sigma_H = 0.5$ ) against the different cases consider here, i.e.  $\Lambda$ CDM-Nx ( $\sigma_H = 1.42$  and  $\sigma_H = 1$ ) and  $\Lambda$ CDM ( $\sigma_H = 1.42, \sigma_H = 1, \sigma_H = 0.5$  and No-Riess for different cosmological parameters. Notice that the change in  $\theta(z_*)$  is quite small and below 0.04% while the changes in  $r_*$  and  $D_A(\star)$  are of the same order and in all cases differ by approximate 1%, corresponding to a percentage change 25 larger than for the  $\theta(z_*)$  quantity. We find a significant decrease in  $\chi^2_{H_0}$  for  $\Lambda$ CDM-Nx ( $\sigma_H = 0.5$ ) compared to all other 6 cases, with a percentage change of  $\Delta P(\chi^2_{H_0}) = -17.44$  against  $\Lambda$ CDM-Nx ( $\sigma_H = 1.42$ ) and  $\Delta P(\chi^2_{H_0}) = -22.21$  against  $\Lambda$ CDM ( $\sigma_H = 1.42$ ), and up to an  $\Delta P(\chi^2_{H_0}) = -38.03$  against  $\Lambda$ CDM-Nx ( $\sigma_H = 0.5$ ). On the other hand we get an increase in

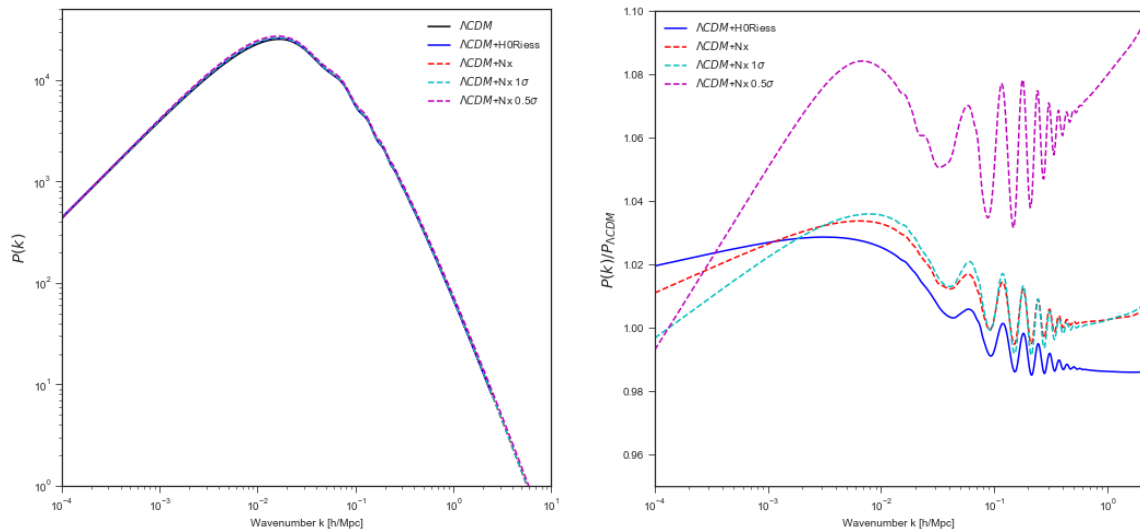


**Figure 5:** We show the matter power spectrum (left panel) for  $\Lambda$ CDM and  $\Lambda$ CDM-Nx and the ratio (right panel)  $\Lambda$ CDM-Nx/ $\Lambda$ CDM and  $\Lambda$ CDM-NoRiess/ $\Lambda$ CDM, where  $1\sigma \equiv 1 \text{ km s}^{-1} \text{ Mpc}^{-1}$  and  $0.5\sigma \equiv 0.5 \text{ km s}^{-1} \text{ Mpc}^{-1}$

percentage difference  $\chi_{cmb}^2$  of at most 0.14% for  $H_0 = 74.03 \pm 05$  with respect to  $\Lambda$ CDM.

## 4.2 Matter Power Spectrum and CMB Power Spectrum

Here we will show the impact in the matter power spectrum of a rapid diluted energy density given by  $\Omega_{ex}(a_c)$  at  $a_c$  with and at a mode  $k_c \equiv a_c H_c$  with  $H_c \equiv H(a_c)$ . As shown in section 3.3 a rapid diluted energy density generates a bump in the ratio of matter power spectrum between  $\Lambda$ CDM-Nx and  $\Lambda$ CDM model [65] and observed in [61, 62], [43, 56, 57, 64, 72–74] and [24, 32, 42]. We show in fig.(5) the matter power spectrum, on the left hand side we plot  $\Lambda$ CDM with and without Riess data [R-19] and the three  $\Lambda$ CDM-Nx ( $\sigma_H = 1.42$ ,  $\sigma_H = 1$ ,  $\sigma_H = 0.5$ ) cases. On the right hand side we show the ratio of  $\Lambda$ CDM-Nx/ $\Lambda$ CDM and  $\Lambda$ CDM-NoRiess/ $\Lambda$ CDM. Notice that for  $\Lambda$ CDM-Nx with  $\sigma_H = 0.5$  we find an increase in power of about 6% for modes  $10^{-3} < k < 1$  in  $\text{h/Mpc}$  units while for the other  $\Lambda$ CDM models ( $\sigma_H = 1.42$  and  $\sigma_H = 1$ ) the difference is below 2%. In fig.(6) we show CMB power spectrum for all five models described above, top panel corresponds to  $C_l^{TT}$  and left bottom panel  $C_l^{TE}$  and  $C_L^{EE}$  right bottom panel.

## 5 Conclusions

We have studied possible solutions to the increasing  $H_0$  tension between local  $H_0$  and Planck CMB measurements in the context of  $\Lambda$ CDM model. Recent local measurements  $H_0$  estimate a value of  $H_0 = 74.03 \pm 1.42 \text{ km s}^{-1} \text{ Mpc}^{-1}$  [1] with a reported average value for different local measurements of  $H_0 = (73.03 \pm 0.8) \text{ km s}^{-1} \text{ Mpc}^{-1}$  [14] while Planck reported value of  $H_0 = (67.36 \pm 0.54) \text{ km s}^{-1} \text{ Mpc}^{-1}$  [9]. The magnitude of the tension between the measurements of early and late time is in the range  $4.0\sigma$  and  $5.7\sigma$  [14], implying an important miss-understanding in either the systematic errors of the observational analysis or may hint towards new physics beyond the concordance cosmological  $\Lambda$ CDM model. Here we take

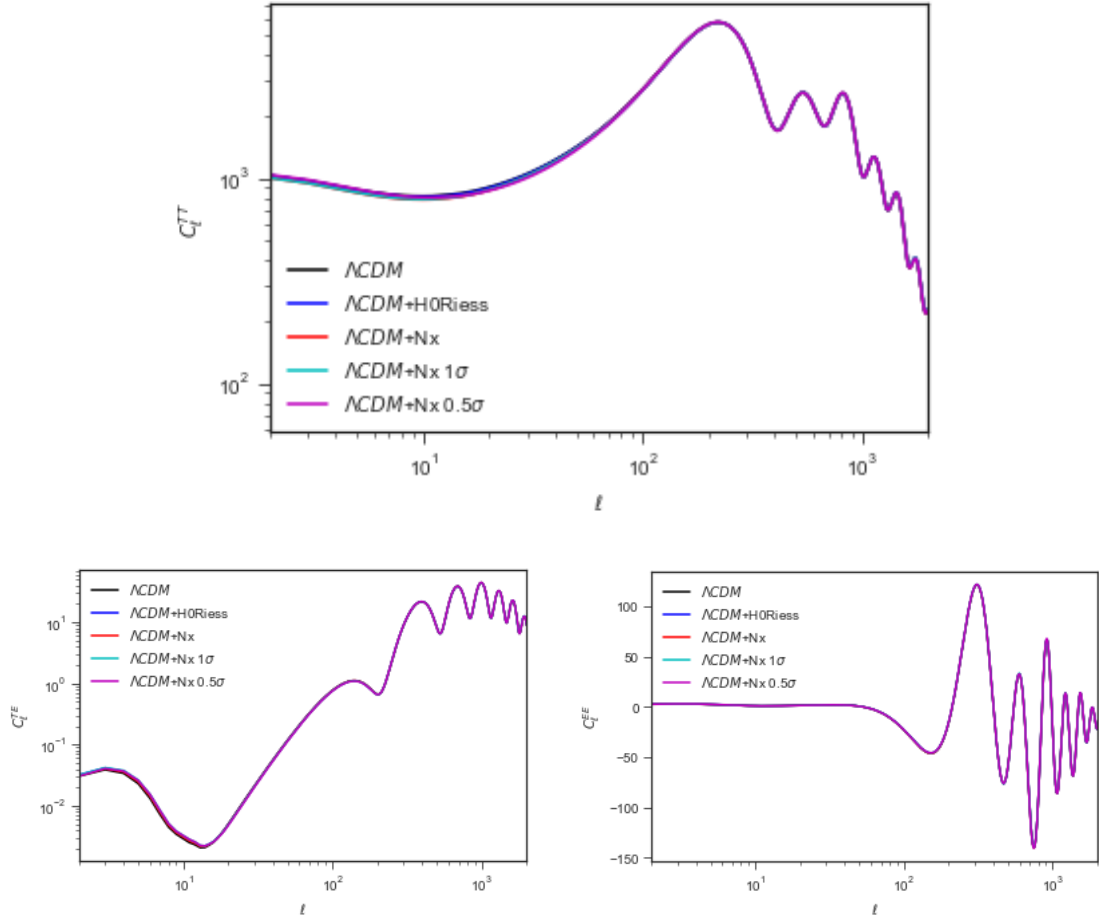


**Figure 6:** We show the CMB-TT power spectrum from  $\Lambda$ CDM-Nx and  $\Lambda$ CDM models and their percentage difference, where  $1\sigma \equiv 1\text{km s}^{-1}\text{Mpc}^{-1}$  and  $0.5\sigma \equiv 0.5 \text{ km s}^{-1}\text{Mpc}^{-1}$ .

the second point of view and study possible solutions to reduce the tension between local  $H_0$  measurements and the Cosmic Microwave Background Radiation observed by Planck satellite. Here we take the second point of view and study possible solutions to reduce the tension between local  $H_0$  measurements and the Cosmic Microwave Background Radiation observed by Planck satellite. Here we have taken this second point of view and we studied models beyond  $\Lambda$ CDM. To alleviate this discrepancy we added to  $\Lambda$ CDM extra relativistic energy density  $\rho_{ex}$  present at early times and we allowed for  $\rho_{ex}$  to dilute rapidly (i.e. as  $\rho_{ex} \propto 1/a^6$ ) for a scale factor larger than  $a_c$  and we named this model  $\Lambda$ CDM-Nx. With these two phenomenological parameters we analyse  $\Lambda$ CDM and  $\Lambda$ CDM-Nx with CMB data and local  $H_0$  measurements. However, besides taking  $H_0 = (74.03 \pm \sigma_H)\text{km s}^{-1}\text{Mpc}^{-1}$  with  $\sigma_H = 1.42$  we also included two forecasting one- $\sigma$  standard deviations values,  $\sigma_H = 1$  and  $\sigma_H = 0.5$ , to assess the impact of these forecasting  $H_0$  measurements on the posteriors probabilities of the different cosmological parameters. We obtained for  $\Lambda$ CDM-Nx with the forecasting local measurement  $H_0 = 74.03 \pm \sigma_H\text{km s}^{-1}\text{Mpc}^{-1}$  with  $\sigma_H = 0.5$  and Planck-2018 CMB (TT,TE,EE+lowE) a value for the Hubble parameter  $H_0 = 72.99 \pm 0.47\text{km s}^{-1}\text{Mpc}^{-1}$  at 68%

c.l. with a best fit  $H_0 = 72.83 \text{ km s}^{-1} \text{ Mpc}^{-1}$ . The relative difference decrease in  $\chi_H^2$  in this  $\Lambda\text{CDM-Nx}$  with respect to  $\Lambda\text{CDM}$  is  $\Delta_{RPD} = 635$  while we obtain a small increase  $\chi_{cmb}$  of  $\Delta_{RPD} = 0.167$ . For the best fits we have a reduction in  $(H_R - H_0)/1.42$  from 4.27 in  $\Lambda\text{CDM}$  to 0.83 for  $\Lambda\text{CDM-Nx}$  ( $sH = 0.5$ ) and the prize to pay is an increase in the percentage difference of 0.14% for the CMB  $\chi_{cmb}^2$ . Finally we would like to stress that our phenomenological model  $\Lambda\text{CDM-Nx}$ , and in particular the  $\rho_{ex}$  and  $a_c$  parameters, may have a sound derivation from extension of the standard model of particle physics as for example BDE or EDE models. These are exiting times to pursue a deeper understanding of our universe in a epoch of high precision observations such as DESI and allows to further constraining the building blocks of particle physics.

## Acknowledgments

A. de la Macorra acknowledges support from Project IN105021 PAPIIT-UNAM, PASPA-DGAPA, UNAM and thanks the University of Barcelona for their hospitality. E. Almaraz acknowledges support of a Postdoctoral scholarship by CONACYT. We also thank M. Jaber and J. Mastache for useful discussions.

## References

- [1] Adam G. Riess, Stefano Casertano, Wenlong Yuan, Lucas M. Macri, and Dan Scolnic. Large Magellanic Cloud Cepheid Standards Provide a 1% Foundation for the Determination of the Hubble Constant and Stronger Evidence for Physics beyond  $\Lambda\text{CDM}$ . *Astrophys. J.*, 876(1):85, 2019. doi: 10.3847/1538-4357/ab1422.
- [2] Boudewijn F. Roukema and Yuzuru Yoshii. The failure of simple merging models to save a flat,  $\Omega_0 = 1$  universe. *Astrophys. J.*, 418:L1–L4, 1993. doi: 10.1086/187101.
- [3] Adam G. Riess et al. Observational evidence from supernovae for an accelerating universe and a cosmological constant. *Astron. J.*, 116:1009–1038, 1998. doi: 10.1086/300499.
- [4] S. Perlmutter et al. Measurements of Omega and Lambda from 42 high redshift supernovae. *Astrophys. J.*, 517:565–586, 1999. doi: 10.1086/307221.
- [5] A. G. Riess, L. M. Macri, S. L. Hoffmann, D. Scolnic, S. Casertano, A. V. Filippenko, B. E. Tucker, M. J. Reid, D. O. Jones, J. M. Silverman, R. Chornock, P. Challis, W. Yuan, P. J. Brown, and R. J. Foley. A 2.4% Determination of the Local Value of the Hubble Constant. *Astrophys. J.*, 826:56, July 2016. doi: 10.3847/0004-637X/826/1/56.
- [6] Adam G. Riess et al. Milky Way Cepheid Standards for Measuring Cosmic Distances and Application to Gaia DR2: Implications for the Hubble Constant. *Astrophys. J.*, 861(2):126, 2018. doi: 10.3847/1538-4357/aac82e.
- [7] Rachael L. Beaton et al. The Carnegie-Chicago Hubble Program. I. An Independent Approach to the Extragalactic Distance Scale Using only Population II Distance Indicators. *Astrophys. J.*, 832(2):210, 2016. doi: 10.3847/0004-637X/832/2/210.
- [8] Wendy L. Freedman et al. The Carnegie-Chicago Hubble Program. VIII. An Independent Determination of the Hubble Constant Based on the Tip of the Red Giant Branch. 7 2019. doi: 10.3847/1538-4357/ab2f73.
- [9] N. Aghanim et al. Planck 2018 results. VI. Cosmological parameters. *Astron. Astrophys.*, 641: A6, 2020. doi: 10.1051/0004-6361/201833910.
- [10] V. Bonvin et al. H0LiCOW – V. New COSMOGRAIL time delays of HE 0435–1223:  $H_0$  to 3.8 per cent precision from strong lensing in a flat  $\Lambda\text{CDM}$  model. *Mon. Not. Roy. Astron. Soc.*, 465 (4):4914–4930, 2017. doi: 10.1093/mnras/stw3006.

- [11] S. Birrer et al. H0LiCOW - IX. Cosmographic analysis of the doubly imaged quasar SDSS 1206+4332 and a new measurement of the Hubble constant. *Mon. Not. Roy. Astron. Soc.*, 484: 4726, 2019. doi: 10.1093/mnras/stz200.
- [12] Kenneth C. Wong et al. H0LiCOW XIII. A 2.4% measurement of  $H_0$  from lensed quasars:  $5.3\sigma$  tension between early and late-Universe probes. 2019.
- [13] P. A. Zyla et al. Review of Particle Physics. *PTEP*, 2020(8):083C01, 2020. doi: 10.1093/ptep/ptaa104.
- [14] L. Verde, T. Treu, and A. G. Riess. Tensions between the Early and the Late Universe. *Nature Astron.*, 3:891, 7 2019. doi: 10.1038/s41550-019-0902-0.
- [15] D.W. Pesce et al. The Megamaser Cosmology Project. XIII. Combined Hubble constant constraints. *Astrophys. J. Lett.*, 891(1):L1, 2020. doi: 10.3847/2041-8213/ab75f0.
- [16] Simone Aiola et al. The Atacama Cosmology Telescope: DR4 Maps and Cosmological Parameters. 7 2020.
- [17] G.E. Addison, Y. Huang, D.J. Watts, C.L. Bennett, M. Halpern, G. Hinshaw, and J.L. Weiland. Quantifying discordance in the 2015 Planck CMB spectrum. *Astrophys. J.*, 818(2): 132, 2016. doi: 10.3847/0004-637X/818/2/132.
- [18] Kevin Aylor, MacKenzie Joy, Lloyd Knox, Marius Millea, Srinivasan Raghunathan, and W.L. Kimmy Wu. Sounds Discordant: Classical Distance Ladder &  $\Lambda$ CDM -based Determinations of the Cosmological Sound Horizon. *Astrophys. J.*, 874(1):4, 2019. doi: 10.3847/1538-4357/ab0898.
- [19] George Efstathiou. H0 Revisited. *Mon. Not. Roy. Astron. Soc.*, 440(2):1138–1152, 2014. doi: 10.1093/mnras/stu278.
- [20] Lloyd Knox and Marius Millea. The Hubble Hunter’s Guide. pages 1–17, 2019. doi: 10.1103/PhysRevD.101.043533.
- [21] Vivian Poulin, Tristan L. Smith, Tanvi Karwal, and Marc Kamionkowski. Early Dark Energy Can Resolve The Hubble Tension. *Phys. Rev. Lett.*, 122(22):221301, 2019. doi: 10.1103/PhysRevLett.122.221301.
- [22] Tanvi Karwal and Marc Kamionkowski. Dark energy at early times, the Hubble parameter, and the string axiverse. *Phys. Rev. D*, 94(10):103523, 2016. doi: 10.1103/PhysRevD.94.103523.
- [23] Jeremy Sakstein and Mark Trodden. Early dark energy from massive neutrinos – a natural resolution of the Hubble tension. *Phys. Rev. Lett.*, 124(16):161301, 2020. doi: 10.1103/PhysRevLett.124.161301.
- [24] Lloyd Knox and Marius Millea. Hubble constant hunter’s guide. *Phys. Rev. D*, 101(4):043533, 2020. doi: 10.1103/PhysRevD.101.043533.
- [25] Eleonora Di Valentino, Alessandro Melchiorri, Olga Mena, and Sunny Vagnozzi. Interacting dark energy in the early 2020s: A promising solution to the  $H_0$  and cosmic shear tensions. *Phys. Dark Univ.*, 30:100666, 2020. doi: 10.1016/j.dark.2020.100666.
- [26] Katherine Freese and Martin Wolfgang Winkler. Chain Early Dark Energy: Solving the Hubble Tension and Explaining Today’s Dark Energy. 2 2021.
- [27] Riccardo Murgia, Guillermo F. Abellán, and Vivian Poulin. Early dark energy resolution to the Hubble tension in light of weak lensing surveys and lensing anomalies. *Phys. Rev. D*, 103(6): 063502, 2021. doi: 10.1103/PhysRevD.103.063502.
- [28] Florian Niedermann and Martin S. Sloth. Resolving the Hubble tension with new early dark energy. *Phys. Rev. D*, 102(6):063527, 2020. doi: 10.1103/PhysRevD.102.063527.

- [29] Eleonora Di Valentino, Olga Mena, Supriya Pan, Luca Visinelli, Weiqiang Yang, Alessandro Melchiorri, David F. Mota, Adam G. Riess, and Joseph Silk. In the Realm of the Hubble tension — a Review of Solutions. 3 2021. doi: 10.1088/1361-6382/ac086d.
- [30] Eleonora Di Valentino et al. Snowmass2021 - Letter of interest cosmology intertwined II: The hubble constant tension. *Astropart. Phys.*, 131:102605, 2021. doi: 10.1016/j.astropartphys.2021.102605.
- [31] J. Colin Hill, Evan McDonough, Michael W. Toomey, and Stephon Alexander. Early dark energy does not restore cosmological concordance. *Phys. Rev. D*, 102(4):043507, 2020. doi: 10.1103/PhysRevD.102.043507.
- [32] Anatoly Klypin, Vivian Poulin, Francisco Prada, Joel Primack, Marc Kamionkowski, Vladimir Avila-Reese, Aldo Rodriguez-Puebla, Peter Behroozi, Doug Hellinger, and Tristan L. Smith. Clustering and Halo Abundances in Early Dark Energy Cosmological Models. *Mon. Not. Roy. Astron. Soc.*, 504(1):769–781, 2021. doi: 10.1093/mnras/stab769.
- [33] Mikhail M. Ivanov, Evan McDonough, J. Colin Hill, Marko Simonović, Michael W. Toomey, Stephon Alexander, and Matias Zaldarriaga. Constraining early dark energy with large-scale structure. *Phys.Rev.D*, 102(10):103502, November 2020. doi: 10.1103/PhysRevD.102.103502.
- [34] Jose Luis Bernal, Licia Verde, and Adam G. Riess. The trouble with  $H_0$ . *JCAP*, 10:019, 2016. doi: 10.1088/1475-7516/2016/10/019.
- [35] Eleonora Di Valentino, Alessandro Melchiorri, Olga Mena, and Sunny Vagnozzi. Nonminimal dark sector physics and cosmological tensions. *Phys. Rev. D*, 101(6):063502, 2020. doi: 10.1103/PhysRevD.101.063502.
- [36] Supriya Pan, Weiqiang Yang, Eleonora Di Valentino, Emmanuel N. Saridakis, and Subenoy Chakraborty. Interacting scenarios with dynamical dark energy: Observational constraints and alleviation of the  $H_0$  tension. *Physical Review D*, 100(10):1–18, 2019. ISSN 24700029. doi: 10.1103/PhysRevD.100.103520.
- [37] Eleonora Di Valentino, Ankan Mukherjee, and Anjan A. Sen. Dark Energy with Phantom Crossing and the  $H_0$  tension. 5 2020.
- [38] Adriá Gómez-Valent, Valeria Pettorino, and Luca Amendola. Update on Coupled Dark Energy and the  $H_0$  tension. 4 2020.
- [39] Guillermo Ballesteros, Alessio Notari, and Fabrizio Rompineve. The  $H_0$  tension:  $\Delta G_N$  vs.  $\Delta N_{\text{eff}}$ . 4 2020.
- [40] Christina D. Kreisch, Francis-Yan Cyr-Racine, and Olivier Doré. The Neutrino Puzzle: Anomalies, Interactions, and Cosmological Tensions. *Phys. Rev. D*, 101(12):123505, 2020. doi: 10.1103/PhysRevD.101.123505.
- [41] Eric V. Linder and Georg Robbers. Shifting the Universe: Early Dark Energy and Standard Rulers. *JCAP*, 06:004, 2008. doi: 10.1088/1475-7516/2008/06/004.
- [42] Matthew J. Francis, Geraint F. Lewis, and Eric V. Linder. Can Early Dark Energy be Detected in Non-Linear Structure? *Mon. Not. Roy. Astron. Soc.*, 394:605–614, 2008. doi: 10.1111/j.1365-2966.2008.14286.x.
- [43] Erminia Calabrese, Roland de Putter, Dragan Huterer, Eric V. Linder, and Alessandro Melchiorri. Future CMB Constraints on Early, Cold, or Stressed Dark Energy. *Phys. Rev. D*, 83:023011, 2011. doi: 10.1103/PhysRevD.83.023011.
- [44] Stephen A. Appleby, Eric V. Linder, and Jochen Weller. Cluster Probes of Dark Energy Clustering. *Phys. Rev. D*, 88:043526, 2013. doi: 10.1103/PhysRevD.88.043526.
- [45] Adam G. Riess et al. New Hubble Space Telescope Discoveries of Type Ia Supernovae at  $z \geq 1$ : Narrowing Constraints on the Early Behavior of Dark Energy. *Astrophys. J.*, 659:98–121, 2007. doi: 10.1086/510378.

- [46] Michael Doran and Georg Robbers. Early dark energy cosmologies. *JCAP*, 06:026, 2006. doi: 10.1088/1475-7516/2006/06/026.
- [47] Rachel Bean, Steen H. Hansen, and Alessandro Melchiorri. Early universe constraints on a primordial scaling field. *Phys. Rev. D*, 64:103508, 2001. doi: 10.1103/PhysRevD.64.103508.
- [48] Paul J. Steinhardt, Li-Min Wang, and Ivaylo Zlatev. Cosmological tracking solutions. *Phys. Rev. D*, 59:123504, 1999. doi: 10.1103/PhysRevD.59.123504.
- [49] Ivaylo Zlatev, Li-Min Wang, and Paul J. Steinhardt. Quintessence, cosmic coincidence, and the cosmological constant. *Phys. Rev. Lett.*, 82:896–899, 1999. doi: 10.1103/PhysRevLett.82.896.
- [50] A. de la Macorra and G. Piccinelli. General scalar fields as quintessence. *Phys. Rev. D*, 61:123503, 2000. doi: 10.1103/PhysRevD.61.123503.
- [51] Axel de la Macorra. A Realistic particle physics dark energy model. *Phys. Rev. D*, 72:043508, 2005. doi: 10.1103/PhysRevD.72.043508.
- [52] A. de la Macorra and C. Stephan-Otto. Natural quintessence with gauge coupling unification. *Phys. Rev. Lett.*, 87:271301, 2001. doi: 10.1103/PhysRevLett.87.271301.
- [53] A. de la Macorra and C. Stephan-Otto. Quintessence restrictions on negative power and condensate potentials. *Phys. Rev. D*, 65:083520, 2002. doi: 10.1103/PhysRevD.65.083520.
- [54] R. R. Caldwell and Eric V. Linder. The Limits of quintessence. *Phys. Rev. Lett.*, 95:141301, 2005. doi: 10.1103/PhysRevLett.95.141301.
- [55] Eric V. Linder. The Dynamics of Quintessence, The Quintessence of Dynamics. *Gen. Rel. Grav.*, 40:329–356, 2008. doi: 10.1007/s10714-007-0550-z.
- [56] Erminia Calabrese, Dragan Huterer, Eric V. Linder, Alessandro Melchiorri, and Luca Pagano. Limits on Dark Radiation, Early Dark Energy, and Relativistic Degrees of Freedom. *Phys. Rev. D*, 83:123504, 2011. doi: 10.1103/PhysRevD.83.123504.
- [57] Johan Samsing, Eric V. Linder, and Tristan L. Smith. Model Independent Early Expansion History and Dark Energy. *Phys. Rev. D*, 86:123504, 2012. doi: 10.1103/PhysRevD.86.123504.
- [58] Ryan E. Keeley, Shahab Joudaki, Manoj Kaplinghat, and David Kirkby. Implications of a transition in the dark energy equation of state for the  $H_0$  and  $\sigma_8$  tensions. *JCAP*, 12:035, 2019. doi: 10.1088/1475-7516/2019/12/035.
- [59] Shadab Alam et al. Completed SDSS-IV extended Baryon Oscillation Spectroscopic Survey: Cosmological implications from two decades of spectroscopic surveys at the Apache Point Observatory. *Phys. Rev. D*, 103(8):083533, 2021. doi: 10.1103/PhysRevD.103.083533.
- [60] Dante V. Gomez-Navarro, Alexander Mead, Alejandro Aviles, and Axel de la Macorra. Impact of cosmological signatures in two-point statistics beyond the linear regime. 9 2020. doi: 10.1093/mnras/staa3393.
- [61] A. de la Macorra and E. Almaraz. Theoretical and Observational Constraints of Bound Dark Energy with Precision Cosmological Data. *Phys. Rev. Lett.*, 121(16):161303, 2018. doi: 10.1103/PhysRevLett.121.161303.
- [62] Erick Almaraz and Axel de la Macorra. Bound dark energy: Towards understanding the nature of dark energy. *Phys. Rev. D*, 99(10):103504, 2019. doi: 10.1103/PhysRevD.99.103504.
- [63] Erick Almaraz, Baojiu Li, and Axel de la Macorra. Nonlinear structure formation in Bound Dark Energy. *JCAP*, 03:016, 2020. doi: 10.1088/1475-7516/2020/03/016.
- [64] Mariana Jaber-Bravo, Erick Almaraz, and Axel de la Macorra. Imprint of a Steep Equation of State in the growth of structure. *Astropart. Phys.*, 115:102388, 2020. doi: 10.1016/j.astropartphys.2019.102388.

- [65] Axel de la Macorra, Dante V. Gomez-Navarro, Alejandro Aviles, Mariana Jaber, Jorge Mastache, and Erick Almaraz. Cosmological signatures of a Rapid Diluted Energy Density. 9 2020.
- [66] Antony Lewis, Anthony Challinor, and Anthony Lasenby. Efficient computation of CMB anisotropies in closed FRW models. *The Astrophysical Journal*, 538:473–476, 2000. doi: 10.1086/309179.
- [67] Cullan Howlett, Antony Lewis, Alex Hall, and Anthony Challinor. CMB power spectrum parameter degeneracies in the era of precision cosmology. *JCAP*, 1204:027, 2012. doi: 10.1088/1475-7516/2012/04/027.
- [68] Antony Lewis. Efficient sampling of fast and slow cosmological parameters. *Phys.Rev.D*, 87: 103529, 2013. doi: 10.1103/PhysRevD.87.103529.
- [69] Antony Lewis and Sarah Bridle. Cosmological parameters from CMB and other data: A Monte Carlo approach. *Phys.Rev.D*, 66:103511, 2002. doi: 10.1103/PhysRevD.66.103511.
- [70] Antony Lewis. GetDist: a Python package for analysing Monte Carlo samples. 2019. URL <https://getdist.readthedocs.io>.
- [71] Ryan E. Keeley, Shahab Joudaki, Manoj Kaplinghat, and David Kirkby. Implications of a transition in the dark energy equation of state for the  $H_0$  and  $\sigma_8$  tensions. *Journal of Cosmology and Astroparticle Physics*, 2019(12):1–17, 2019. ISSN 14757516. doi: 10.1088/1475-7516/2019/12/035.
- [72] Mariana Jaber and Axel de la Macorra. Probing a Steep EoS for Dark Energy with latest observations. *Astropart. Phys.*, 97:130–135, 2018. doi: 10.1016/j.astropartphys.2017.11.007.
- [73] Mariana Jaber and Axel de la Macorra. Constraints on Steep Equation of State for the Dark Energy using BAO. 4 2016.
- [74] N. Chandrachani Devi, M. Jaber-Bravo, G. Aguilar-Argüello, O. Valenzuela, A. de la Macorra, and H. Velázquez. Non-linear Structure Formation for Dark Energy Models with a Steep Equation of State. *JCAP*, 09:050, 2020. doi: 10.1088/1475-7516/2020/09/050.